



VIDEO SENSOR SYSTEM ANALYSIS REPORT

L. A. Lalumiere

Ocean Sciences Division
Maritimes Region
Fisheries and Oceans Canada

Bedford Institute of Oceanography
P.O. Box 1006
Dartmouth, Nova Scotia
Canada B2Y 4A2

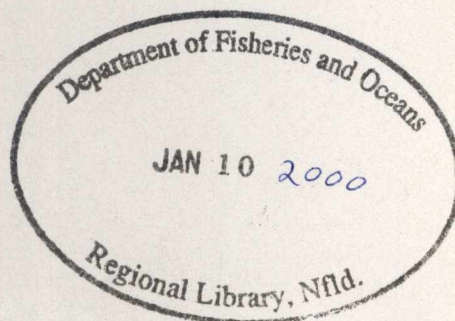
1999

Canadian Contractor Report of Hydrography and Ocean Sciences 55



Fisheries
and Oceans

Pêches
et Océans



Canada

Canadian Contractor Report of
Hydrography and Ocean Sciences 55

1999

Video Sensor System Analysis Report

by

L. A. Lalumiere*

Ocean Sciences Division
Maritimes Region
Fisheries and Oceans Canada

Bedford Institute of Oceanography
P.O. Box 1006
Dartmouth, Nova Scotia
Canada B2Y 4A2

*Sensors by Design Ltd., 217 Lorne Avenue, Newmarket, Ontario, L3Y 4K5
This report was prepared under DSS Contract No. F5955-8-0282, funded
through the Federal Panel of Energy, Research and Development.

© Public Works and Government Services 1999
Cat. No. Fs 97-17/55E ISSN 0711-6748

Correct Citation for this publication:

Lalumiere, L.A. 1999. Video Sensor System Analysis Report. Can. Contract.
Rep. Hydrogr. Ocean Sci. 55: ix + 71 p.

TABLE OF CONTENTS

ABSTRACT	v
RÉSUMÉ	vi
LIST OF FIGURES	vii
LIST OF TABLES	ix
1 INTRODUCTION	1
1.1 VIDEO SENSOR SYSTEM DESCRIPTION.....	1
2 SENSOR ALIGNMENT AND RESAMPLING	7
2.1 ANALYSIS DATA SET DESCRIPTION.....	7
2.2 GPS POSITIONS.....	10
2.3 VIDEO FRAME POSITIONING.....	11
2.4 LASER AND VIDEO POSITIONING	21
3 VIDEO ANALYSIS	26
3.1 VIDEO IMAGE BRIGHTNESS PROFILE AND LASER ALTIMETER PROFILE.....	26
3.2 VIDEO MULTI-SPECTRAL ANALYSIS.....	28
3.3 VIDEO IMAGE PLOTTING	35
4 ICE PARAMETER MEASUREMENT	41
4.1 ICE FLOE SIZE MEASUREMENT	41
4.2 ICE CONCENTRATION MEASUREMENT	57
4.3 ICE ROUGHNESS MEASUREMENT	58
5 CONCLUSIONS AND RECOMMENDATIONS	58
6 REFERENCES	60
APPENDIX A. VIDEO DISTORTION CORRECTION EXAMPLE	61

APPENDIX B. LASER POINTER METHOD FOR LASER ALTIMETER/VIDEO ALIGNMENT	62
APPENDIX C. CONTRIBUTION OF RADARSAT SUB-PIXEL SCALE ICE PROPERTIES TO THE SAR BACKSCATTER PAPER.....	63

ABSTRACT

Lalumiere, L.A. 1999. Video Sensor System Analysis Report. Can. Contract. Rep. Hydrogr. Ocean Sci. 55: ix + 71 p.

Various processing and display techniques have been applied to the data collected with the Video Sensor System developed for the Bedford Institute of Oceanography. This helicopter-mounted system collects digital video images, laser altimeter profiles and radar altimeter profiles with GPS positioning. The Video Sensor System is designed for use on Canadian Coast Guard helicopters where it collects data unobtrusively during ice reconnaissance flights. This report documents the analysis performed on data collected with the Video Sensor System near PEI in March 1998 and in March 1999.

A description of the various components in the Video Sensor System along with the performance of the various sensors is provided. Also, ice features that can be determined from the video system and examples of various types of hardcopy presentation and archive print-outs are provided. The results of processing the Video Sensor System data for ice parameters such as floe and lead size, ice concentration and ice roughness are presented.

As a result of this analysis work, the parameters and display techniques that are ready for incorporation in a field display program are:

- GPS flight track positions
- Flying height
- Laser ice roughness
- Quick look video plots
- Geo-referenced video plots.

The following items require further development to make them ready for either scientific or operational use:

- Video frame mosaicking for plots and extracting a brightness profile.
- Video image colour processing for ice cover
- Automatic ice floe size and ice concentration measurements

RÉSUMÉ

Lalumiere, L.A. 1999. Video Sensor System Analysis Report. Can. Contract. Rep. Hydrogr. Ocean Sci. 55: ix + 71 p.

Diverses techniques de traitement et d'affichage ont été appliquées aux données recueillies au moyen du système de capteurs vidéo développé pour l'Institut océanographique de Bedford. Ce système monté sur hélicoptère recueille des images vidéo numériques, des profils altimétrique laser et des profil altimétriques radar avec un dispositif de positionnement GPS. Le système de capteurs vidéo est conçu en vue d'être monté sur des hélicoptères de la Garde côtière canadienne, où il recueille des données sans nuire au reste des activités durant des vols de reconnaissances des glaces. La présente documente l'analyse faite des données recueillies avec le système de capteurs vidéo près de l'Î.-P.-É. en mars 1998 et en mars 1999.

On trouvera dans la présente une description des diverses composantes du système de capteurs vidéo, ainsi que du rendement des divers capteurs utilisés. On y montre aussi les caractéristiques de la glace qui peuvent être déterminées au moyen du système vidéo, ainsi que des exemples des divers types de présentations papier et d'imprimés à archiver que l'on peut produire. On y présente aussi des résultats du traitement des données du système de capteurs vidéo qui servent à déterminer les paramètres des glaces, par exemple les dimensions de la glace de banc et des chenaux libres, la concentration des glaces et leur rugosité.

Suite au travail d'analyse, les paramètres et les techniques d'affichage qui sont prêts à être intégrés au programme d'affichage sur le terrain sont :

- les positions GPS des routes de vol
- l'altitude du vol
- la rugosité de la glace déterminée au laser
- les vues par vidéo rapides
- les vues par vidéo géoréférencées

Les éléments suivants devront être peaufinés avant que l'on puisse les utiliser à des fins scientifiques ou opérationnels :

- Mosaïque de cadres vidéo pour les visualisations et l'extraction d'un profil de luminance
- Traitement d'images vidéo en couleurs pour la couverture de glace
- Mesures automatiques de la taille de la glace de banc et de la concentration de la glace.

LIST OF FIGURES

Figure 1.1.1 An example of the directory structure used to hold the captured images.....	5
Figure 1.1.2 An example directory listing of captured images.	5
Figure 1.1.3 Photograph of the pod mounted to the helicopter.....	7
Figure 2.1.1 GPS track for lines 3 and 4 from March 11, 1998.....	8
Figure 2.1.2 Video frames over Seatrout Point from line 4.....	9
Figure 2.3.1 Eight images from line 132, collected on March 17, 1998 at an average altitude of 46.1m, which provides an average image width of 49.3m.....	13
Figure 2.3.2 Mosaic close-up showing common points and centre of images. Axes are in pixel units (1 pixel=0.154m using a flying height of 46.1m).....	14
Figure 2.3.3 Mosaic of 8 image from line 132 flown on March 17, 1998. The mosaic has a total length of approximately 245m and a width of 49.3m. The axes are in pixel units (.154m/pixel).	16
Figure 2.3.4 Frame-to-frame distance track for manual, automatic and GPS methods. Both the manual and cross-correlation methods use a fixed flying height (though this may not be the case).....	17
Figure 2.3.5 Example of subscene from first (source) image and scan area in second image (showing automatically-located matching area).....	18
Figure 2.3.6 Eight subscenes from first image pair with indicated results.....	19
Figure 2.3.7 Frame overlap measured using the manually-determined common points.....	21
Figure 2.4.1 Plot of laser altimeter and radar altimeter profiles from line 507 flown on March 19, 1998. At a flight speed of 50m/sec the plot shows altimeter data profile of approximately 7km in length.	23
Figure 2.4.2 Line 4 laser profile with close-up over Seatrout Point.....	24
Figure 2.4.3 GPS position of video frames and laser points over Seatrout Point	25
Figure 3.1.1 Laser roughness and image brightness profiles.	27
Figure 3.2.1 Plot of image count 251 from line 47 (flown on March 1, 1999) showing the area within the frame used for the colour analysis.....	28
Figure 3.2.2 Plot of RGB mean values along line 47 (averaged over a small area of image).....	32
Figure 3.2.3 Plot of RGB standard deviation (STD) values along line 47 (averaged over a small area of image).	32
Figure 3.2.4 Plot of HSV mean values along line 47 (averaged over a small area of image).....	33
Figure 3.2.5 Plot of HSV standard deviation (STD) values along line 47 (averaged over a small area of image).	33
Figure 3.2.7 Plot of NTSC YIQ standard deviation (STD) values along line 47 (averaged over a small area of image).	34
Figure 3.3.1 Quick-look plot for line 47 (D1999_060F047) collected on March 1, 1999 at a nominal altitude of 50 m. The line length is approximately 14.9 km.....	36

Figure 3.3.2 Geo-referenced plot for line 47 (D1999_060F047) collected on March 1, 1999 at a nominal altitude of 50 m.....	38
Figure 3.3.3 Geo-referenced plot for line 49 (D1999_060F049) collected on March 1, 1999 at a nominal altitude of 300 m.....	39
Figure 3.3.4 Geo-referenced plot with a map base for line 86 (D073F086) collected on March 14, 1998 f at a nominal altitude of 2500 m.....	40
Figure 4.1.1 Plot of the original gray-scale images used for the floe size measurements.....	42
Figure 4.1.2 Matlab graphical user interface developed for manual floe size measurements.....	43
Figure 4.1.3 Plot of 10 images with an overlay of the manually-digitized floe outlines.....	44
Figure 4.1.4 Histograms of floe size.....	45
Figure 4.1.5 Plot of 10 images with a grey-scale coding to indicated the floes identified by the connected components analysis for the automatic floe size processing routine.....	51
Figure 4.1.6 Histograms of floe size.....	52

LIST OF TABLES

Table 3.2.1 Manual interpretation of surface ice features for line 47 (D1999_060F047) collected on March 1, 1999.....	31
Table 4.1.1 Ice Concentration results	58

1 INTRODUCTION

This report documents the analysis performed on data collected with the BIO Video Sensor System. The analysis documents the performance of individual sensors which comprise the Video Sensor System and the results when a combination of sensors are used. The analysis work used the data set collected near PEI in March 1998 (Sensors by Design, 1998) and data collected in March 1999.

The first section of the report provides a description of the various components in the Video Sensor System. The second section describes the performance of the various sensors individually and when combined. The third section looks at the ice features that can be determined from the video imagery and provides examples of video presentation plots. The fourth section reports performance of the system for the quantitative measurement of ice parameters such as floe and lead size, ice concentration and ice roughness.

1.1 VIDEO SENSOR SYSTEM DESCRIPTION

The BIO Video Sensor System is helicopter-mounted and collects digital video images, laser altimeter profiles and radar altimeter profiles with GPS positioning. The system is designed for use on Canadian Coast Guard BO-105 helicopters. It is composed of a laptop computer, a small power/signal distribution box and a pod which mounts to the helicopter's skid gear. The pod houses a video camera and a laser altimeter. The video sensor system uses the helicopter's on-board radar altimeter and GPS navigation system. The system collects data unobtrusively during ice reconnaissance flights, recording the flight path and data from several sensors monitoring the ice surface.

1.1.1 Video Camera

The Video Sensor System uses a Sony DXC-107A video camera. The camera's white balance settings can be fixed for outdoor use. This is an important feature as a fixed color balance will keep the relative brightness between the red, green and blue components of the image constant and will not change with the light source or the colors in the image.

This camera has an electronic shutter speed control that removes the need for an auto-iris lens. The electronic shutter can respond to image brightness changes quickly, reducing image distortion when the image scene changes from dark open water to bright snow-covered ice.

The camera's video output signal can be standard composite video or s-video.

The video camera's 6 mm lens has a horizontal field of view of 56.1 degrees and a vertical field of view of 43.6 degrees. The typical size of the captured video frames is 320 by 240 pixels (picture elements), though other sizes can be captured, such as 640 by 480 pixels and 160 by 120 pixels. With the 56.1 degree horizontal field of view, the width of the image seen at the surface is equal to 1.07 times the flying height of the sensor system. With a vertical field of view of 43.6 degrees, the height of the image seen at the surface is equal to 0.8 times the flying height of the sensor system. Flying at a survey height of 300m, the width of the image on the surface is 320m for an image pixel size of 1 m by 1 m.

For a wider field of view, the system has been tested with a 4.2 mm lens. This lens has a horizontal field of view of 75 degrees and a vertical field of view of 58.6 degrees. This lens was used during the last two days of the 1998 field trial and was used for the long video survey flown with the *Ice Probe* system on March 19, 1998 (Holladay and Prinsenber, 1999).

The 6mm lens has a small amount of spherical distortion. The 4.2 mm wide angle lens has substantial distortion. Appendix A has a short report documenting the distortion with the 4.2 mm lens and a technique to correct it.

The video camera is mounted in the external pod. A glass port-hole protects the camera from outside weather conditions.

1.1.2 GPS Receiver

Trimble TNL-3100 is part of the on-board equipment on Coast Guard BO-105 helicopters.

The standard output string contains the following relevant parameters:

Latitude (dd mm.mm)
Longitude (ddd mm.mm)
Flight track (degrees - ddd)
Ground speed (knots - kkk)
Date (mm/dd/yy)
Time (hh:mm:ss)

When the extended message output is enabled (by selecting output format X0) the follow parameters are also provided:

Extended Latitude (dd mm.mmmmm)
Extended Longitude (ddd mm.mmmmm)
Extended Ground Speed (kkk.k)
GPS Altitude (ff,fff.f)

Extended solution time (hh:mm:ss.sss)
GPS mode and number of satellites

1.1.3 Laser Altimeter

An Optech G-150 laser altimeter is mounted in the external pod. A glass port-hole protects the laser from outside weather conditions. Glass used for the port-hole is type B-270 manufactured by Schott Glass Technologies Inc.

Laser altimeter specifications from Optech G-150 manual:

Range: 0.2 m to greater than 100 m.
Resolution: 1 cm
Accuracy +/- 5 cm from 10 Celsius to 30
Accuracy +/- 10 cm from -20 Celsius to 50

Beam divergence: 5/1000 (or 0.3 degrees)
Wavelength: 890 nm

Output rate slow: fast:
Feet or meter output display

Weight: 1.2 kg
Dimensions: 70 mm H by 115 mm W by 175 mm D
Input power: 12 VDC nominal (9.5 –15V)
Current Consumption: 0.75 A at 12 v (9 W)

Operating Temperature: –10 to +50
Storage: –40 to +50
Humidity: 0 to 95 %, non-condensing

1.1.4 Radar Altimeter

Specifications for the helicopter's on-board radar altimeter (King KRA-405) were obtained from Transport Canada.

The altimeter operates using FM-CW modulation with a center frequency of 4300 MHz, with 100 MHz peak-to-peak FM modulation with a nominal modulation frequency of 100 Hz. Transmitter power is reported to be 150 mW.

The reported accuracy for the radar altimeter is 3 percent at ranges less than 500 feet (152 m) and 5 percent at ranges greater than 500 feet. The reported resolution is 0.48 feet (0.15 m).

The analog precision equipment output provides altitude proportional to -10 mV per foot over a range from -20 feet to 2500 feet with zero feet equal to 0.0 volts. The analog output has been filtered to have a 0.1 second time constant.

The radar antenna's beamwidth is 50 degrees and separate antennas are used for transmit and receive.

1.1.5 Logging System

1.1.5.1 Hardware

The logging system hardware is based upon a Panasonic CF-25 laptop computer. This laptop computer has a Pentium 166 MHz CPU, 48 megabytes of RAM and 6.4 gigabyte hard-disk. This laptop is built for use in harsh environments. A key feature of this laptop is its three PC-Card slots for data input cards. PC-Cards are used for video capture (Nogatech Capture-Vision card model NV-256), analog input to digitize the radar altimeter signal (Computer Boards Inc's model PCM-DAS16/16) and an additional RS-232 serial port (Socket Communications' model R-I/O ruggedized serial I/O card). A Smartronix Inc. strain relief device is mounted to the side of the laptop to protect the connections to the PC-Cards.

1.1.5.2 Software

The logging program has been developed using Microsoft Visual Basic Version 5.0. The logging program has a video preview window to display the captured images from the video camera. Fields show the current outputs from the GPS receiver, the laser altimeter and the radar altimeter.

The logging software logs data from each device asynchronously. A packetized data file stores data from each device as it arrives with a time-stamp from the computer's on-board clock. Each video frame is stored in its own file. All of the various sensors' data values are stored separately in the ancillary data file.

The logging program stores the following packets in the ancillary data file:

- the parameter file as a packet (one only per file)
- GPS positions (1 per second)
- radar altimeter readings (20 samples per second)
- laser readings (approximately 30 samples per second)
- video frame number (at whatever period the frame interval is set to)

The filenames are created automatically each time logging starts. The ancillary data file name starts with the letter d, followed by the Julian day followed by the letter f, followed by the file number. The file's extension is ".GPS". For example, the name for the ancillary data file collected on March 12 (Julian day 071), and file number 36 is "D071F036.GPS". The video frames (Windows 3.0 bitmap format) are stored in a subdirectory structure starting with a directory that follows the similar naming structure as the ancillary data file, except that the first letter is V. The directory name for the file number 36 collected on March 12 is "V071F036". The files reside below this directory in subdirectories based on the hour and minute (from the data logger system clock) the images were captured (this limits the number of images in any directory to several hundred or less). An image captured at 8:53 AM on March 12 would be located in the directory structure shown in Figure 1.1.1.

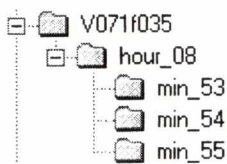


Figure 1.1.1 An example of the directory structure used to hold the captured images.

The video image file names are created using a frame number that continuously increments. An example directory listing is shown in Figure 1.1.2.

Contents of 'S:\V071F035\hour_08\min_53'			
Name	Size	Type	Modified
i0000425.bmp	226KB	Bitmap Image	3/12/98 8:53 AM
i0000426.bmp	226KB	Bitmap Image	3/12/98 8:53 AM
i0000427.bmp	226KB	Bitmap Image	3/12/98 8:53 AM
i0000428.bmp	226KB	Bitmap Image	3/12/98 8:53 AM
i0000429.bmp	226KB	Bitmap Image	3/12/98 8:53 AM
i0000430.bmp	226KB	Bitmap Image	3/12/98 8:53 AM
i0000431.bmp	226KB	Bitmap Image	3/12/98 8:53 AM
i0000432.bmp	226KB	Bitmap Image	3/12/98 8:53 AM

Figure 1.1.2 An example directory listing of captured images.

1.1.5.3 Frame rate and image overlap

The same ice feature will only be seen in the next video frame if the video capture interval is short enough to provide overlapping coverage. Typical settings for overlap are 30 to 40 percent. The logging program has a dialog box which guides the operator on the selection of the video frame rate based on expected flying height, flying speed, camera and lens specifications and the desired frame overlap.

1.1.5.4 Operational considerations for hard disk space.

The typical captured image size is 320 by 240 pixels. As the images are in 24 bit colour format, each images uses 230,454 bytes of hard disk storage space. When the flying height is 50 m the frame capture interval is typically 0.5 seconds. When the flying height is 300 m the frame capture interval is typically 3 seconds.

Hard disk storage space is used up at a rate of 1.6 gigabytes per hour when flying at 50 m and at a rate of 300 megabytes per hour when flying at 300 m. A typical two hour survey flight with a half hour logging at 50 m, one hour logging at 300 m and a half hour used for ferrying will consume 1.1 gigabytes of hard-disk space. The system uses one gigabyte IOMEGA Jaz disks for archiving the data at the end of a survey flight. The data logger currently has 5 gigabytes of space available for survey data collection.

1.1.5.5 Automatic data logging

For the 1999 field trial an automatic logging capability was added to the system. The required video capture frame rate is determined on-the-fly using radar altimeter flying height and GPS-determined ground. Automatic logging poses the problem of data files and directories becoming too large for the back up Jaz disks. To keep the volume of data in any one sub-directory structure the automatic logging mode toggles restarts logging with a new file directory name on a timed basis (for example every 20 minutes) or by altitude (when flying height goes above 700 feet to perform an *Ice Probe* background measurement).

1.1.6 External Pod

The video camera and laser altimeter are mounted in an external pod attach to the helicopters skid gear. The pod was designed by Transport Canada in 1993 so that a video camera could be used with the *Ice Probe* system. For the Video Sensor System, the pod has been modified slightly to add removable glass port holes for the laser altimeter and video camera. Figure 1.1.3 shows a photograph of the pod mounted to the helicopter.

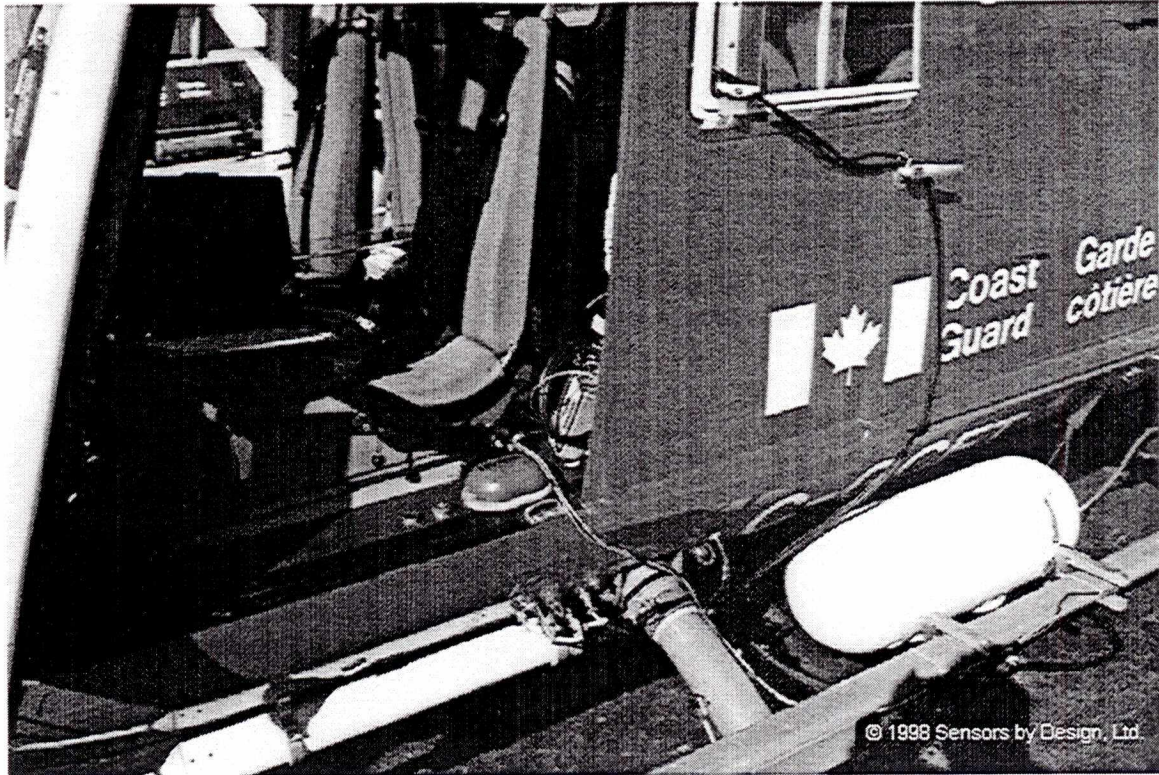


Figure 1.1.3 Photograph of the pod mounted to the helicopter.

2 SENSOR ALIGNMENT AND RESAMPLING

2.1 ANALYSIS DATA SET DESCRIPTION

The first test flight of the Video Sensor System with the laser altimeter added was on March 11, 1998. This flight left the Coast Guard hangar at the Charlottetown airport and flew out over Hillsborough Bay. Line 3 flew from the harbour narrows out over Governors Island at a target altitude of 50 m and a video frame interval of 0.5 seconds. Line 4 circled around in Hillsborough Bay and returned to Charlottetown harbour at a target altitude of 100 m and a video frame interval of 1 second. GPS tracks for lines 3 and 4 are plotted in Figure 2.1.1.

The video frames of the approach to and departure from Governors Island (frame numbers 461 to 484 from Line 3) show straight shoreline features making it impractical to locate landfall on a topographic map. Line 4's flight into the harbour narrows shows the crossing of two points, Seatrout Point and Battery Point. Seatrout Point can be seen in the sequence of video frames from 960 to 962 (see Figure 2.1.2). Battery Point can be seen in the sequence of video frames from 987 to 990.

Part of line 4 near Seatrout Point was selected for several parts of the analysis documented below.

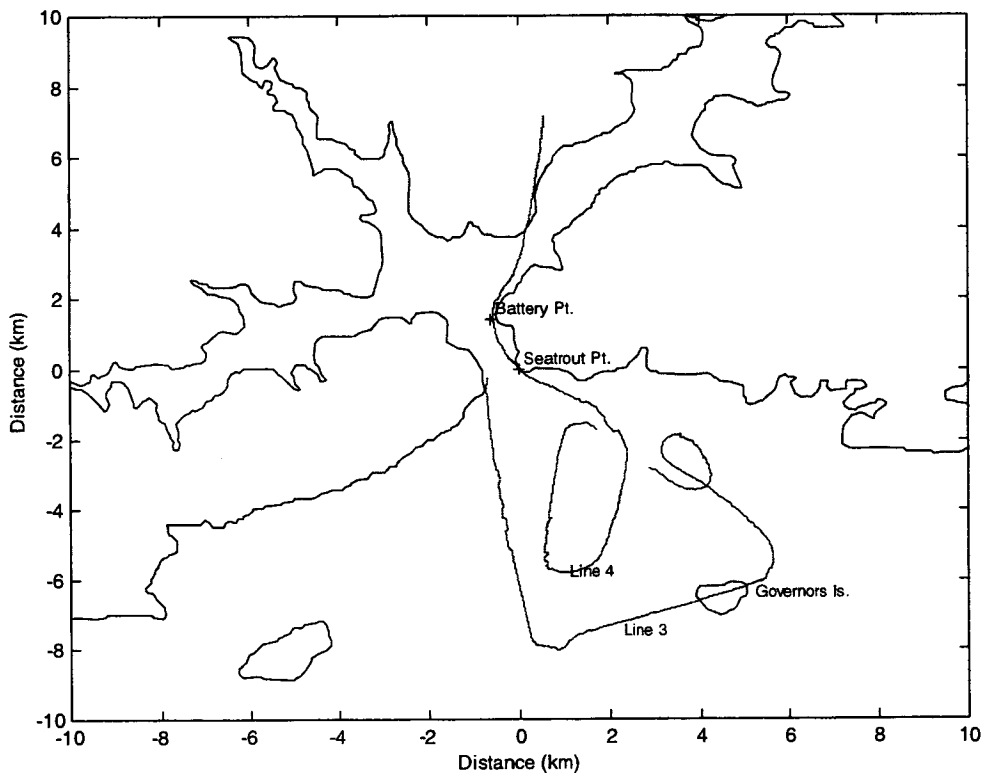


Figure 2.1.1 GPS track for lines 3 and 4 from March 11, 1998

2.1.1 Topographic Map Positions

Universal Transverse Mercator (UTM) coordinates for Seatrout Point and Battery Point were obtained from the Charlottetown 1:50000 topographic map. UTM coordinates from the topographic map are in NAD27 coordinate units (NAD27 datum shift with the Clarke 1866 spheroid). For comparisons with the airborne GPS data, coordinates taken from the topographic map are converted using a FORTRAN subroutine called GSULCONV which is part of the Ice Probe system software. A Matlab MEX program was made to access the subroutine from the Matlab command window.

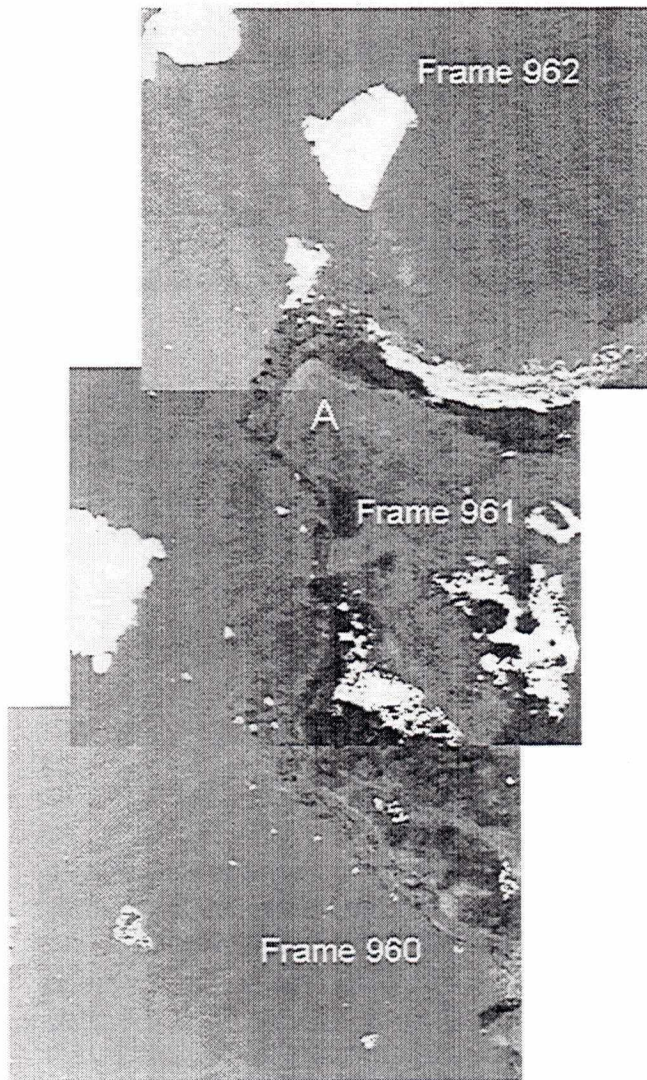


Figure 2.1.2 Video frames over Seatrout Point from line 4

2.1.2 Digital Shoreline Data

A public domain shoreline database was found at the website of the School of Ocean and Earth Science and Technology (SOEST) at the University of Hawaii. The database is called "GSHHS - A Global Self-consistent, Hierarchical, High-resolution Shoreline Database". Quoting from the website (<http://www.soest.hawaii.edu/wessel/gshhs/gshhs.html>): "GSHHS is a high-resolution shoreline data set amalgamated from two data bases in the public domain". The database is available for download at <ftp://kiawe.soest.hawaii.edu/pub/wessel/gshhs> or <ftp://ftp.ngdc.noaa.gov/MGG/shorelines/>.

The full-resolution worldwide shoreline database is approximately 90 megabytes in size. Lower resolutions are available, but for this work a high resolution shoreline limited to the region of the Gulf of St. Lawrence in the vicinity of PEI was required.

By modifying the example program 'gshhs.c' provided at the FTP site, programs to window the full-resolution database and convert it to a Matlab readable text file were written. The resulting file for the area around PEI is approximately 900 kilobytes in size.

The online documentation for the GSHHS database did not specify the spheroid or datum shift. Trial and error tests indicated that it is probably WGS 84, but the locations of Seatrout Point and Battery Point in the digital database did not line up with the topographic coordinates for those points. A small correction was applied to the GSHHS database so that the digital shoreline would line up fairly well with the points taken from the topographic map.

2.2 GPS POSITIONS

2.2.1 GPS Noise and Filtering.

Digital filters were developed to clean up the GPS position information collected with the Coast Guard helicopter's Trimble TNL3100 GPS receiver. GPS position fixes are provided at a rate of approximately 1 Hz. Approximately every 45 seconds the GPS time provided with the position would skip one second, though the distance traveled from the previous position fix did not double. Also, the time stamp applied by the logging program did not show any anomalies around the GPS-time jump. It is apparent that the GPS time stamp provided with the position fix (with is limited to integer values) does not have sufficient resolution and the position fix rate is actually 2 percent slower than the expected rate of 1 Hz.

The data string from the GPS receiver has a resolution of 0.01 minutes (of latitude or longitude). The dominant noise source appears to be caused by the coarse resolution and manifests itself as either several duplicate latitude values when the flight track is in a mostly east or west direction or several duplicate longitude values when the flight track is in a mostly north or south direction.

Fine detail can be preserve by applying a filter which cuts off completely at a data point frequency of slightly less than $0.25 * \text{sampling rate}$. The logic for this filter is based on techniques used to filter first-order hold methods of interpolation.

Some other noise sources are a few garbled positions that can be picked out easily and a few 50 m offsets in the data which are probably caused by a change in the selection of satellites used by the GPS receiver to calculate the position.

Some offsets are temporary (lasting 2 to 3 seconds) and some appear as an offset with no apparent return.

A brief check was made to determine if the short term GPS position offsets (caused by the loss of view of satellites low on the horizon) could be removed. The GPS receiver calculated velocity and heading are logged in the Video Sensor System data set. A vector of distance traveled between each GPS data point was created and converted to instantaneous velocity. A comparison between the GPS receiver-calculated velocity and the instantaneous velocity calculated from the GPS positions showed a good match except for large spikes in the instantaneous velocity at the point where the GPS positions showed offsets. If in the future there is a need to remedy these offsets, it appears that a technique could probably be developed.

2.2.2 GPS Position Interpolation

The GPS positions were interpolated to a sample rate of 100 Hz. This rate provides easy alignment with other data channels such as the laser altimeter. The original GPS time values were a problem due to their one second resolution. The time stamps provided by the logging system have a 55 ms resolution and have some jitter. A new channel of time stamp values were created by finding the start and end GPS times for a line, calculating the actual sampling interval by dividing the elapsed time by the number of GPS positions and generating a new time channel using the calculated sampling interval. A time channel with 0.01 second interval was created from the start time of a line to the end time. The Matlab routine *Interp1* was used to interpolate the latitude values and the longitude values independently (or UTM northing and easting values independently).

2.2.3 GPS Accuracy

Relative GPS positioning accuracy is in the range of 50 m. The dominate noise source limiting the relative accuracy appears to be the offsets noted above.

From the laser altimeter and video frame positioning work documented below, the absolute accuracy was found to be approximately 50 m.

2.3 VIDEO FRAME POSITIONING

The digital video data is a useful source of information about the sea ice cover, but helicopter motion and the unknown amount of overlap between frames has made extracting information from the video data difficult. Common features seen in adjacent images can be used to determine how far the helicopter has traveled

and the relative change in heading direction. The distance between the centres of the adjacent images and a measure of the helicopters heading change can then be used to plot the video frames as a continuous image swath as shown in Figure 2.3.3.

This video frame positioning analysis first prepares a reference data set collected by manually locating common features in consecutively collected images. This is followed by the description of an automatic technique to determine alignment of consecutive images using a cross correlation technique. In addition to the above, frame positioning using interpolated GPS positions are determined.

The final result for this section provides a comparison of frame-to-frame overlap calculated using the three positioning techniques (manual, automatic and GPS-based).

2.3.1 Selected Video Sequence

For the frame distance offset measurements, a sequence of frames taken near the Confederation Bridge were used, specifically frames 34681 to 34696 from line 132, which was flown on March 17, 1998. Over this short section the mean laser altimeter provided flying height was 46.1 m for an image pixel size of 0.154 m. This sequence was chosen as there was some overlapping coverage of the ice surface from one image to the next. The first eight frames of the sequence are shown in Figure 2.3.1.

2.3.2 Manual Frame-to-Frame Distance Measurements

Well-defined ice features were located in adjacent video images. Typically, the feature in the first image is near the top of the image. As the helicopter travels forward, the same ice feature can be seen near the bottom of the subsequent image. Using the computer's mouse, the pixel coordinates of the feature in the first image was found. Next, the coordinate of the same feature in the second image was found. The same ice feature will only be seen in the next video frame if the video capture interval is short enough to provide overlapping coverage.

For the manual measurements, two common features were selected for each pair of adjacent images. One feature was selected from the left side and one from the right side. The wide separation of the points provides a good estimate of the slope of a line drawn between the two points. The slope of the line between the two points in the first image plus the slope of the line between the two points in the second image provides a measure of the rotation of the camera (and the helicopter) from one frame to the next.

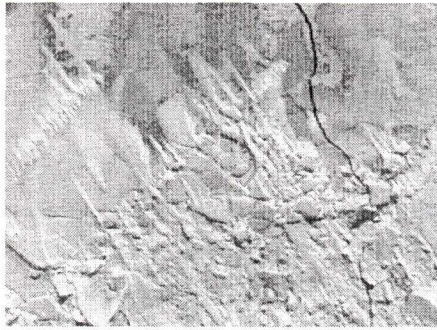


Image i0034681

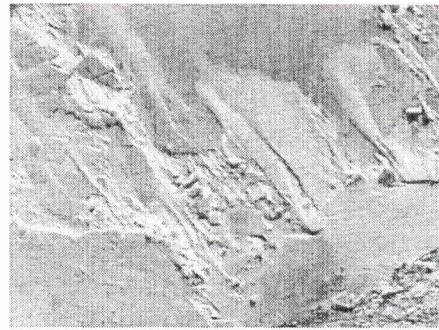


Image i0034685

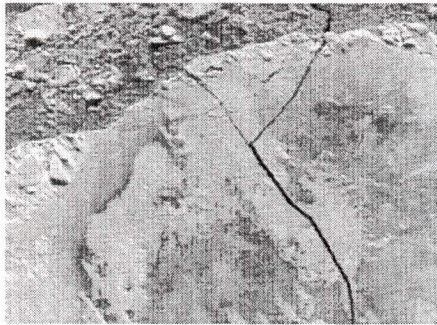


Image i0034682

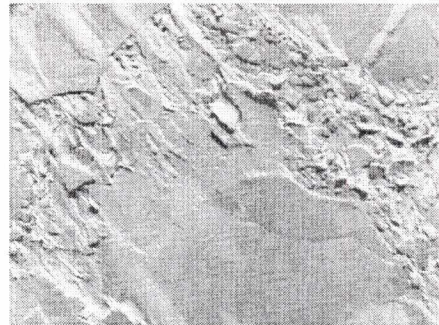


Image i0034686

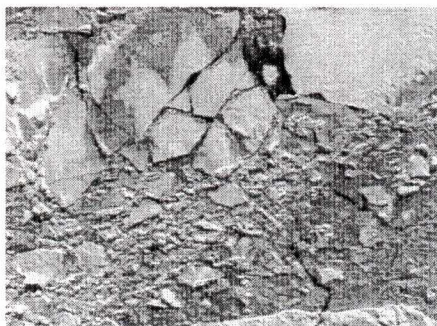


Image i0034683

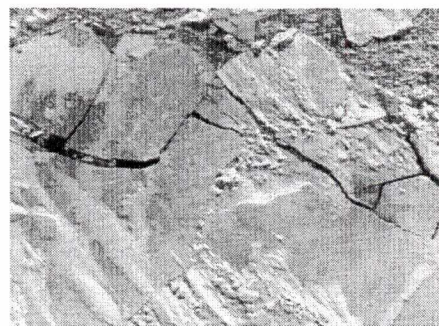


Image i0034687

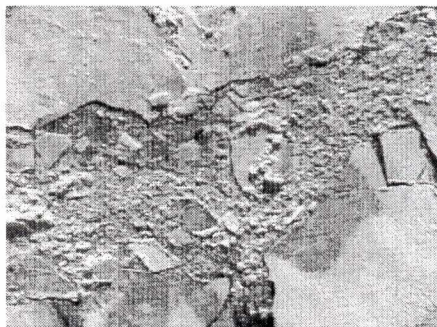


Image i0034684

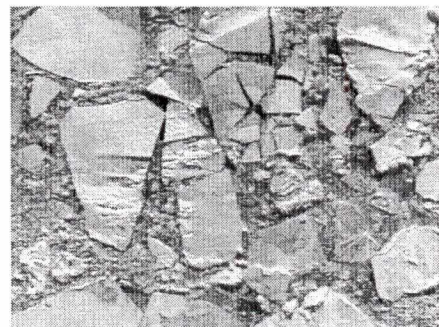


Image i0034688

Figure 2.3.1 Eight images from line 132 collected on March 17, 1998 at an average altitude of 46.1m, which provides an average image width of 49.3m

With common features located and the rotation angle between frames measured, the number of pixels from the centre of the first frame to the centre of the second can be calculated. Flying height obtained from the laser altimeter can be used to convert the pixel separation to a distance in metres.

Figure 2.3.2 shows two images mosaicked together using the manually located common points. Manually located common features are marked with '+' symbols. The image centres are marked with 'x' symbols. Boxes are plotted to indicate the perimeter of the images.

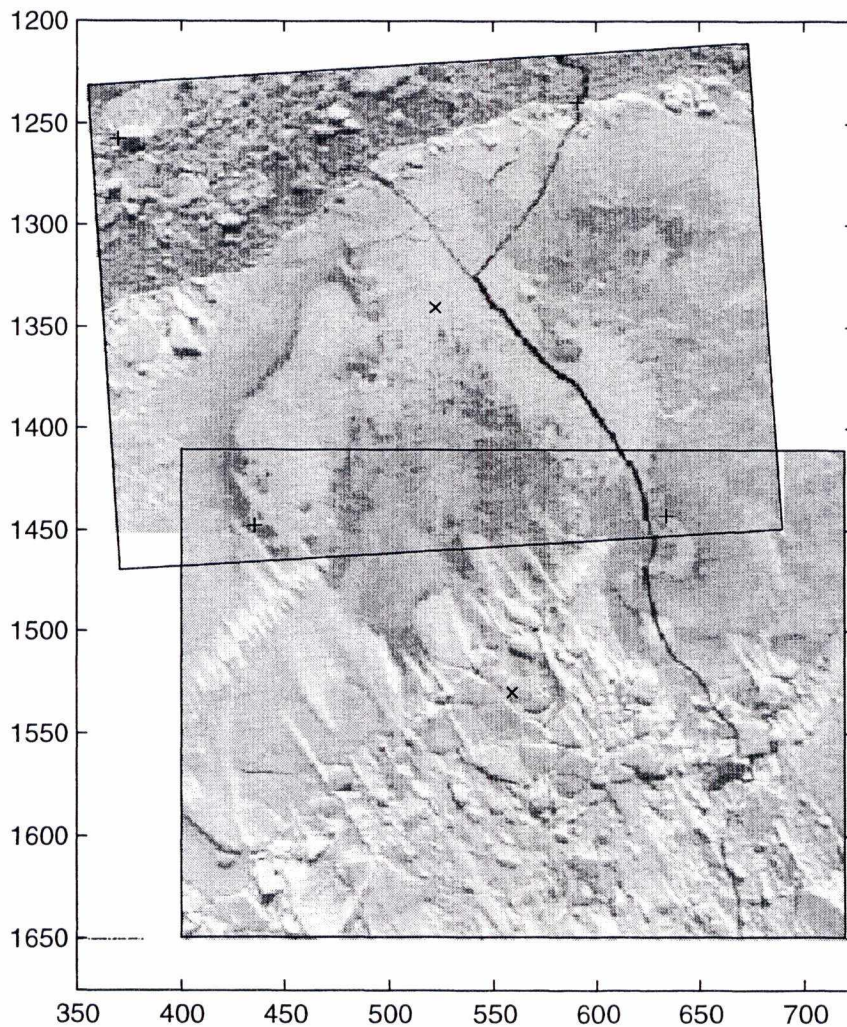


Figure 2.3.2 Mosaic close-up showing common points and centre of images. Axes are in pixel units (1 pixel=0.154m using a flying height of 46.1m).

Figure 2.3.3 shows a mosaic made from the first 8 images selected for this analysis. There are a few artifacts in the mosaic caused by the simple method used to overlay the images. The images were placed one on top of each other in a Matlab array (large enough to hold all the images) using simple Matlab array indexing which transfers large amount of data with a single command. More complicated (and slower running) Matlab code is required for the creation of an artifact-free mosaic.

Common features were found in 15 pairs of images. Figure 2.3.4 shows a plot of frame-to-frame distance track, along with the results from the automated image matching and the GPS positions (both described below).

2.3.3 Automatic Frame-to-Frame Distance Measurements

An algorithm for semi-automatic frame-to-frame offset measurements was developed. The algorithm uses two-dimensional cross-correlation measurements on sub-sections of adjacent images. The algorithm implemented is not optimal nor is it 100% effective in all cases, but it does provide sufficient quantity and quality of results to evaluate the utility of the technique.

When image collection rate is high enough to provide overlapping coverage, features seen in the top of the first image (of a pair of adjacent images) can be seen near the bottom of the second image. The processing algorithm extracts a 32 by 32 pixel subscene from the first image. An area in the second image is selected over which the subscene from the first image will be cross-correlated. For each cross-correlation, each subscene has its mean value subtracted. The Matlab cross-correlation function returns a two dimensional matrix, from which the maximum value is located and saved for comparison with other cross-correlation results.

To locate a matching area in the second image, the first image is swept over an area in the second image. A two-dimensional cross-correlation matrix is created with the value from each correlation placed in the matrix location corresponding to the location of the subscene in the second image. After all the cross-correlations have been performed, the location of the maximum value in the cross-correlation matrix is found. This location can be positioned relative to the top right corner of the image and comparing this position with the position of the subscene in the first image, an estimate of helicopter motion from frame to frame can be made (assuming the video downward orientation does not alter between frames).

To test the implementation and provide results for this analysis, 8 subscenes were compared on a series of 15 pairs of images.

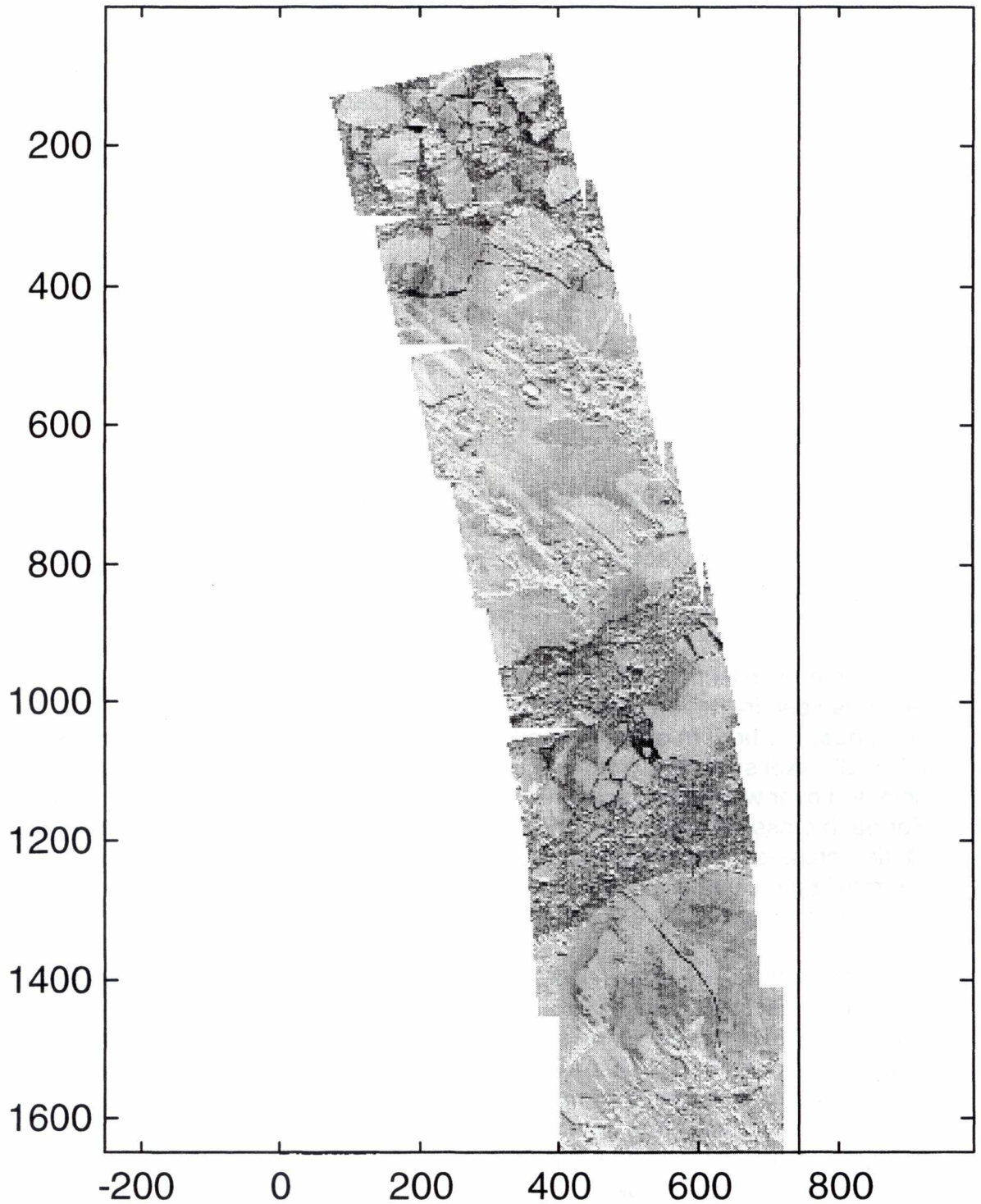


Figure 2.3.3 Mosaic of 8 images from line 132 flown on March 17, 1998. The mosaic has a total length of approximately 245m and a width of 49.3m. The axes are in pixel units (.154m/pixel).

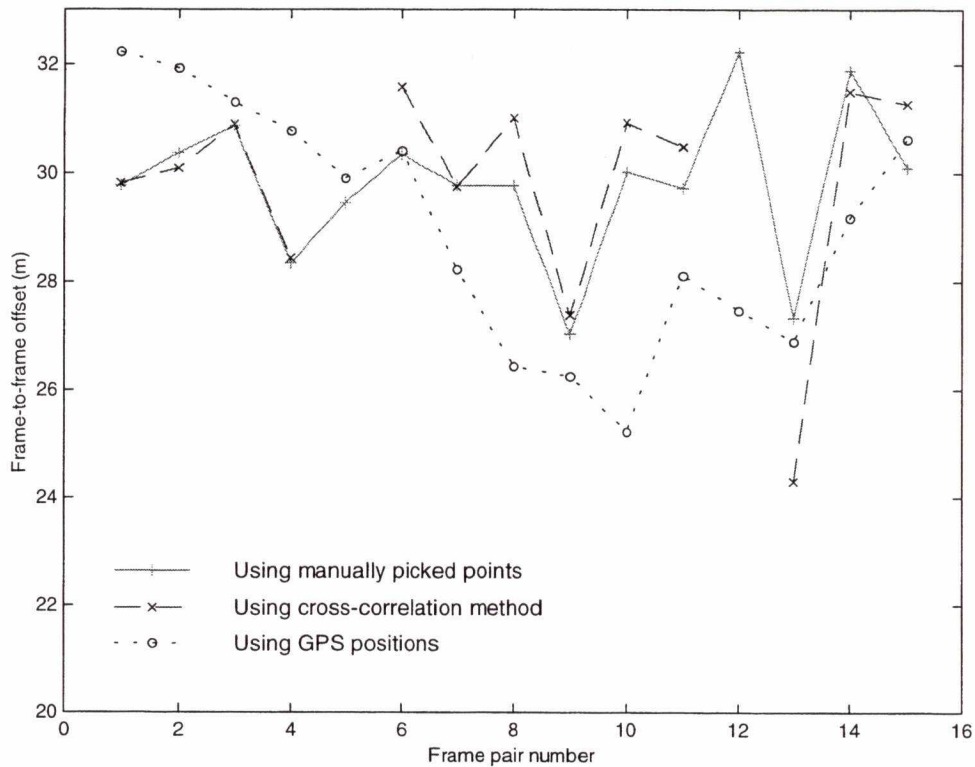


Figure 2.3.4 Frame-to-frame distance track for manual, automatic and GPS methods. Both the manual and cross-correlation methods use a fixed flying height (though this may not be the case).

Figure 2.3.5a shows an example first image with the subscene area marked. Figure 2.3.5b shows the second image used. The larger box in Figure 2.3.5b indicates the area which is swept over. The small box indicates the automatically-located matching subscene. Figure 2.3.6 shows the 8 subscenes from the first image (of an example pair of images) and the automatically-located subscenes in the second image. Subscenes 2, 3 and 4 did not match up, but the rest did. Comments on subscene matching are placed beside each subscenes pair in the figure.

The technique is semi-automatic at this time, as the results had to be evaluated manually to determine if the located subscenes were correct. For the 15 pairs of images, 5 pairs had correctly located all 8 subscenes, for one image pair no matches were found, and between 4 to 7 subscenes were matched in the remaining pairs of images. The image offset measurements were selected only from the manually-chosen correct results.

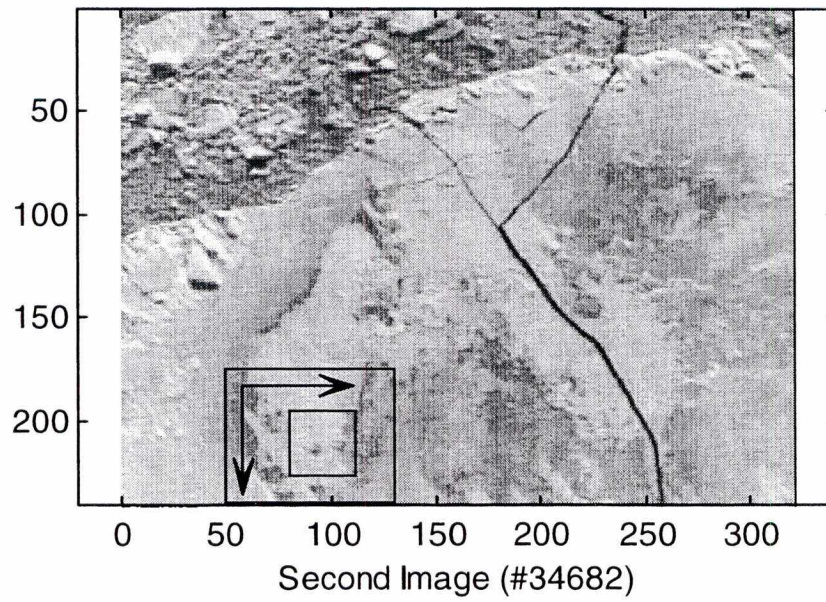
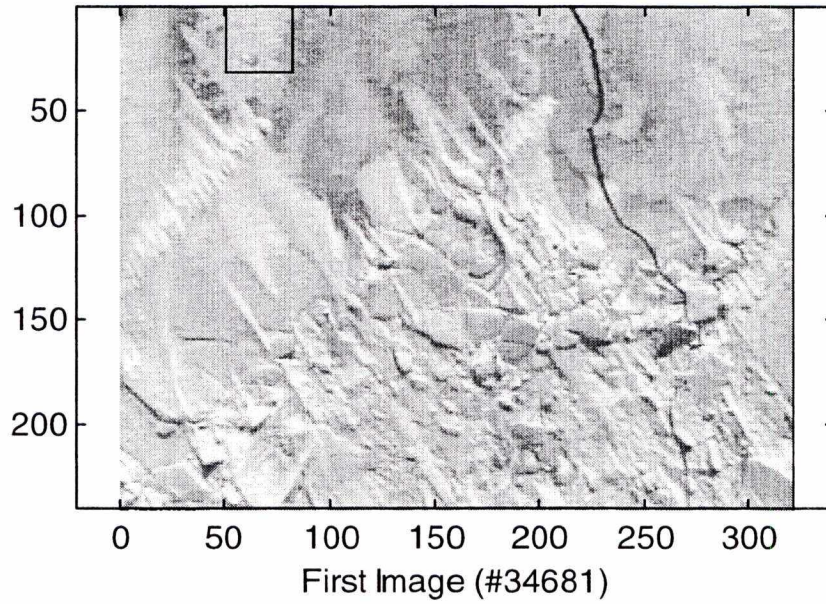


Figure 2.3.5 Example of subscene from first (source) image and scan area in second image (showing automatically-located matching area).










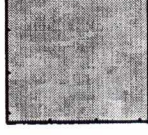






First	Second	Results
		Good Match
		No Match
		No Match
		No Match
		Good Match
		Good Match
		Good Match
		Good Match

Figure 2.3.6 Eight subscenes from first image pair with indicated results.

2.3.4 GPS-Based Frame-to-Frame Distance Measurements

GPS positions for line 132 were filtered following the method described above in section 2.2.1 and interpolated to a sample rate of 100 Hz. The time stamps for the 15 video frames used in the above analysis were used to look up the GPS position for each video frame. The positions were converted to UTM coordinates so that the distance traveled from frame to frame could be measured. The results are shown in Figure 2.3.4. The standard deviation between the GPS-based frame-to-frame distance traveled and the manually-measured frame-to-frame distance traveled is 2.3 m (for an image series collected at a flying height of approximately 45 m).

2.3.5 Frame Overlap

Actual overlap from the manually-measured frame-to-frame distance traveled is shown in Figure 2.3.7. This overlap is based on the distance from the centre of each frame and the 'height' of the image. Overlap towards the sides of the image may be more or less. The average overlap value is approximately 20 percent – which is less than the value that was expected. The logging system was configured to capture a frame every 0.5 seconds but the actual logging interval is in the range of 0.65 seconds to 0.7 seconds. (The longer interval is due to the nature of timer event used in the logging program to trigger frame collection. For 1999 this problem was reduced.)

An overlap of 20% means that the ice seen in the top 50 pixels of one image will appear in the bottom 50 pixels of the next image.

From the above section the standard deviation of the error in GPS-based frame-to-frame distance traveled is 2.3 m which is an error of approximately 15 image pixels. Overlap based on GPS positions will be over- or under-estimated by 30%.

The error in the GPS-based frame-to-frame distance measurement is very small compared to expected GPS positioning errors. As the GPS positions for the video frames are determined by looking up the video frame's time-stamp in the interpolated GPS position data, video frame time-stamping errors must be small.

Another source of uncertainty in the GPS positioning for the video frames is helicopter pitch and roll. For example, if the helicopter is pitching forward by 5 degrees, then the centre of the video image will be 4.4 m behind the expected position (assuming level flight).

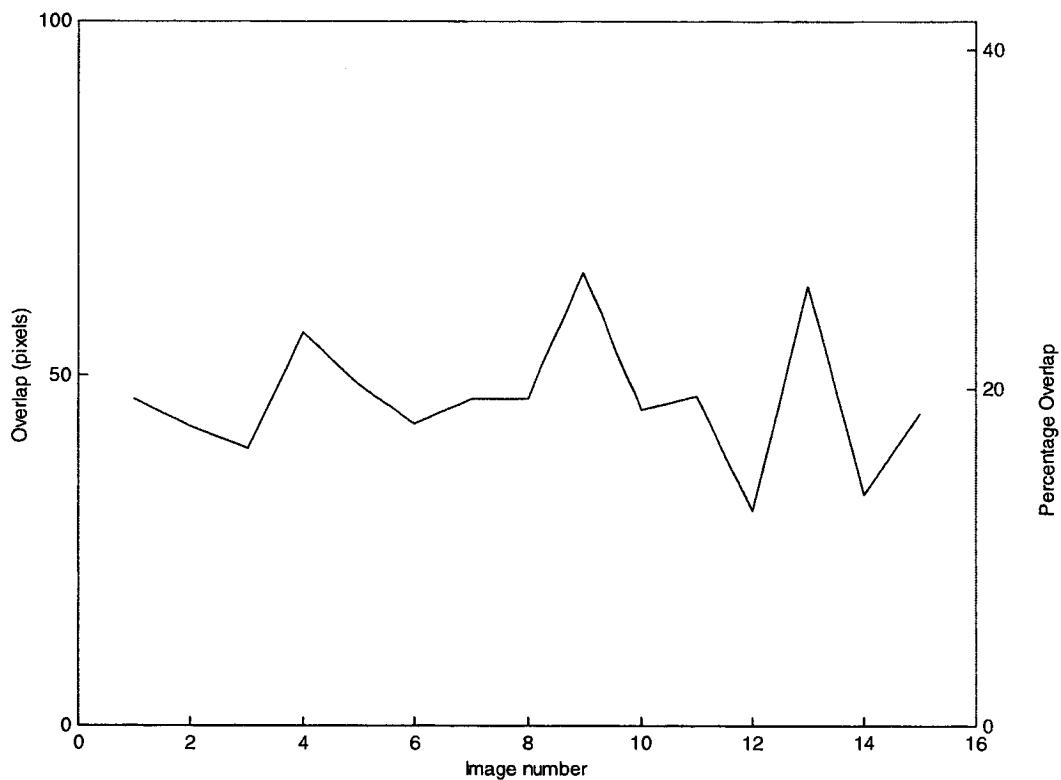


Figure 2.3.7 Frame overlap measured using the manually-determined common points.

2.4 LASER AND VIDEO POSITIONING

2.4.1 Laser and Radar Altimeter Positioning

2.4.1.1 Pitch and roll effects in the laser altimeter readings

Laser has a pencil-like beam with a width of 0.3 degrees. If the helicopter is pitching forward by approximately 8 degrees, the altitude reported by the laser will be 0.5m greater than the actual flying height. The BO-105 helicopter flies with a downward pitch compared to the angle when on the ground. The laser is mounted in the pod with a slight forward angle to compensate for the helicopter's flying attitude. At present the Video Sensor System does not have pitch and roll sensors, so the magnitude of pitch- and roll-induced noise cannot be estimated.

2.4.1.2 Pitch and roll effects in the radar altimeter readings

The size of the radar's footprint on a rough, planar surface varies with flying height (Annan and Davis, 1977). The footprint radius ranges from approximately $1/40^{\text{th}}$ of the flying height at 50m to $1/100^{\text{th}}$ of the flying height at 300m (1.32m and 3.25m foot print radii respectively).

With the 50 degree beam width of the radar altimeter's antenna pattern, the range reported will not vary with pitch and roll under normal flying conditions.

2.4.1.3 Radar altimeter alignment with laser altimeter

The radar altimeter signal has a noise problem that was not corrected until the afternoon of March 17, 1998, so only the surveys on March 18 and March 19 have useable radar altimeter data.

A plot was made of laser altimeter flying height and radar altimeter flying height for line 507 flown following the western side of the Confederation Bridge on March 19, 1998. The plot is shown in Figure 2.4.1. The radar altimeter noise levels are 3 percent of the reading (when flying less than 500 feet), so the expected noise level of 1.5 m agrees with the noise in radar altimeter data seen in the plot. The laser altimeter height tracks the radar altimeter height quite well, but the radar altimeter reading are generally higher than the laser. The laser altimeter heights and the radar altimeter heights differ by as much as 2 m.

The laser altimeter reading increases with helicopter pitch. Also, on the BO-105 helicopter, the radar altimeter is mounted on the bottom side of the helicopter's tail boom behind the helicopter's centre of mass. As the pod (with the video camera and laser altimeter) is mounted ahead of the helicopter's centre of mass, downward helicopter pitch changes will raise the tail boom relative to the pod increasing the radar altimeter reading.

The difference in height reading may be due to a combination of helicopter pitch increasing the laser altimeter reading and downward helicopter pitch increasing the radar altimeter reading. With the combined effects, the helicopter would have to pitch down 21 degrees for 2 m difference to occur. In Figure 2.4.1, the radar altimeter reading appears to be greater than the laser reading throughout the survey line. This indicates that the radar must be greater than the laser in level flight.

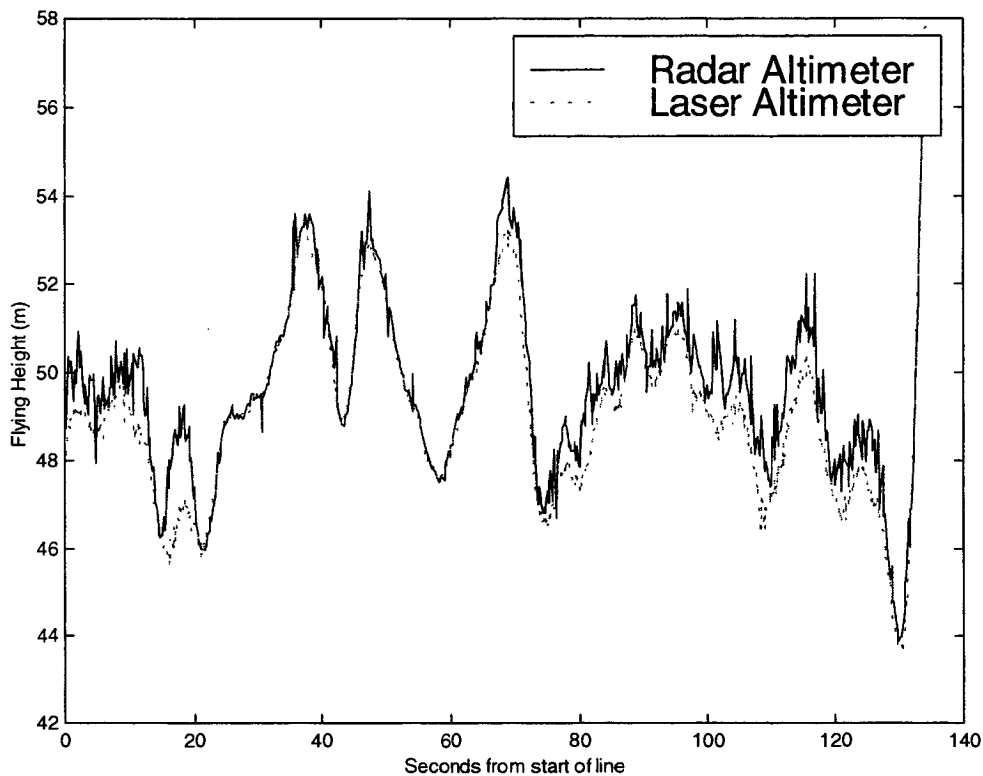


Figure 2.4.1 Plot of laser altimeter and radar altimeter profiles from line 507 flown on March 19, 1998. At a flight speed of 50m/sec the plot shows an altimeter data profile of approximately 7km in length.

2.4.2 Matching Features with the Laser and Video Images

For this analysis a section of line 4 (on March 11, 1998) near Seatrout Point was used. Figure 2.1.2 shows three video frames (960, 961 and 962). The video frame capture interval for this line is 1 second and the nominal flying height over the point was 78m. With the video camera's 56.1 degree horizontal field of view, the width of the image at the ground surface is approximately 83m. The width of the tip of Seatrout Point is estimated to be 20m.

On the approach to and the departure from Seatrout Point, Hillsborough Bay and the harbour narrows were ice-free. The laser altimeter reading was lost for most of the open water section but the tip of Seatrout Point was profiled (see feature marked A in Figure 2.1.2). The upper part of Figure 2.4.2 shows the laser altimeter profile plot for line 4. The plot shows interpolated laser values where laser drop-outs occurred when flying over areas of open water. The lower part of Figure 2.4.2 shows a close-up of the laser altimeter profile plot over the tip of Seatrout Point. The laser has been interpolated to a rate of 100 Hz and the

helicopter's velocity reported by the GPS receiver is 55 m/s. As there are 36 interpolated laser points over the point of land, the estimated width of the land feature profiled by the laser is 20 m.

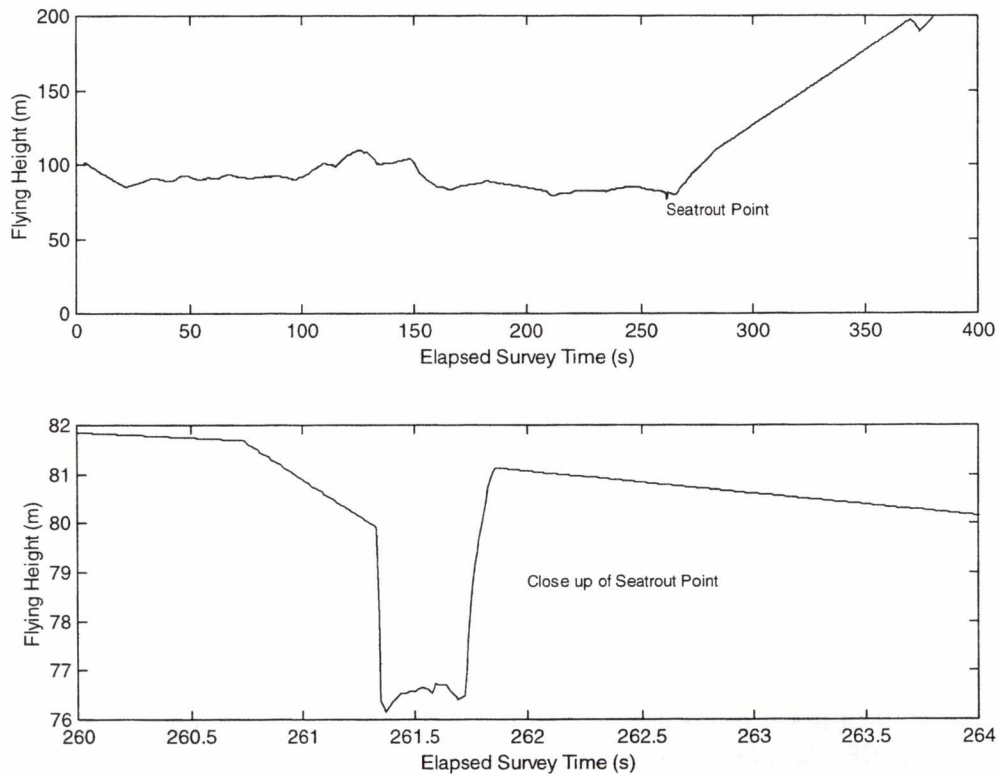


Figure 2.4.2 Line 4 laser profile with close-up over Seatrout Point.

As the width of the tip of Seatrout Point measured from the video frames and the width estimated from the laser profile are similar, there is some confidence that the same feature has been detected with both sensors.

Appendix B describes a calibration technique added for the 1999 field trial which positions the laser altimeter's ground contact point within the video frame.

2.4.3 Positioning Accuracy of Video Frames Versus Laser Altimeter Data.

Figure 2.4.3 shows a plot of the helicopter's GPS track from line 4 in the area of the narrows of Charlottetown harbour. The positions marked with an 'x' indicate the centre location of the video frames. The positions marked with a '+' indicate the positions of the processed and interpolated laser points.

Time stamps for the video frames should represent the time that the camera is over the centre of the image. From Figure 2.1.2, the tip of Seatrout Point can be seen at the top of image 961 and at the bottom of 962. The end time of the laser profile over the tip of the point should have been passed one half of a second before the collection of frame 962, but from Figure 2.4.3 the start of the laser profile over the tip starts midway between frames 961 and 962. As the elapsed time of the laser profile over the tip of the point is 0.36 seconds the laser points appear to be out of position by 20m.

The reason for this misalignment (though small) is unknown, but a likely cause is a small misalignment between the look angle of the camera and the direction the laser is pointing. If the current misalignment were entirely due to the difference in the video camera's and laser's look angle, this angle would be approximately 14 degrees. Appendix B describes a technique to align the laser altimeter and video camera in the hangar prior to mounting the pod on the helicopter.

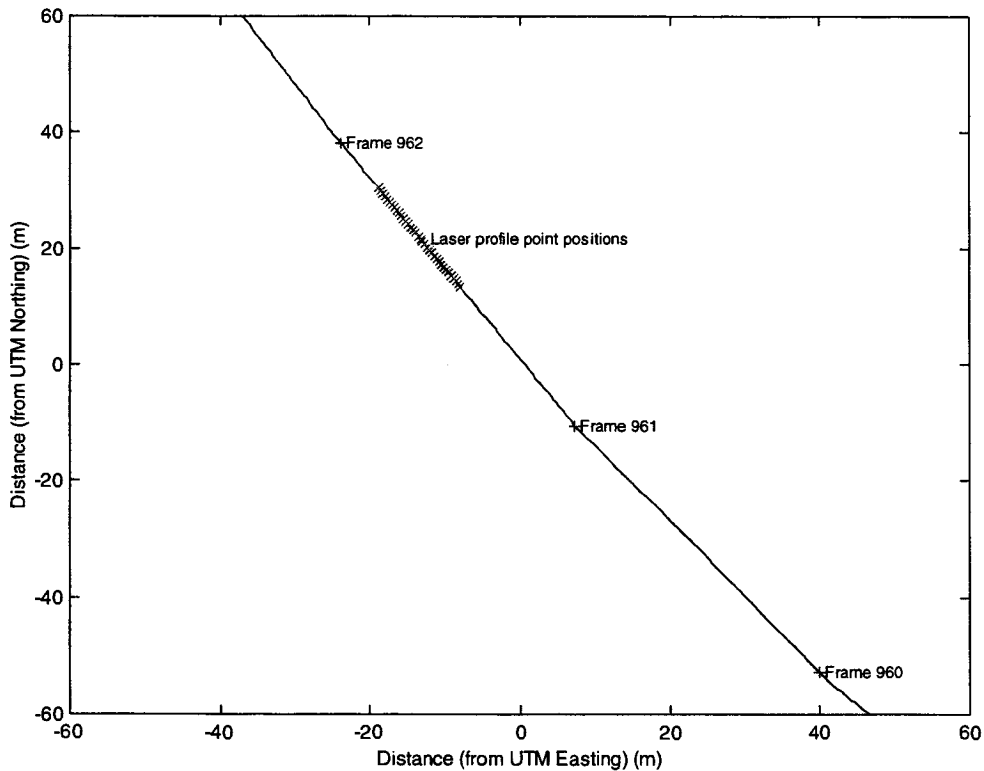


Figure 2.4.3 GPS position of video frames and laser points over Seatrout Point

3 VIDEO ANALYSIS

There is a wide range of ice conditions encountered. Some examples of ice conditions are listed below.

Images with only ice:

- only ice which is part of one large thick floe.
- only thin newly-formed ice with possible rafting.
- many floes distinguished by rough edges
- all rubble ice
- all ice but with varying thicknesses

The above examples can have varying amounts of open water. Further variations can be obtained by changes in cloud cover, sun angle and flying height. The image series used in the following sections represent a subsection of all the images available.

3.1 VIDEO IMAGE BRIGHTNESS PROFILE AND LASER ALTIMETER PROFILE

An image brightness profile was extracted from the image mosaic made from the March 17 survey near the Confederation Bridge (shown in Figure 2.3.3). The brightness profile is plotted in Figure 3.1.1b. The profile starts at the bottom of the mosaic and follows the centre of the mosaic up to the top. The extracted brightness profile follows a straight line from the centre point of each image. The x-axis scale is in pixel number as extracted from the centre of the mosaicked image.

A difference function (Matlab function `diff.m`) was applied to the brightness profile and the results are plotted in Figure 3.1.1c. The *differenced* brightness function clearly shows areas that are smooth and areas that are rough. Very small floes seen at the top of image i0034682 (the individual images are shown in Figure 2.3.1) and the bottom half of image I0034683 can be seen as a large response in the area of pixel numbers 350 to 500. From pixel numbers 500 to 600, the brightness difference response is low; this is over the white medium-sized floes seen near the top of image I0034683. The very small floes seen in image I0034684 have a large response in the brightness difference profile from pixel numbers 600 to 800. The flat area of ice seen at the top of image I0034685 and the lower half of image I0034686 can be seen as a small response in the brightness difference profile from pixel numbers 850 to 1050.

The laser altimeter ice roughness measurement profile is included as part a) of Figure 3.1.1. A visual comparison between the laser roughness profile and the

image brightness profile does not show much in common between the two. The laser altimeter provides a direct measure of ice roughness, but as the laser is sampling at approximately 30 Hz, the ground sample spacing is approximately one sample every 1.7m.

Changes in the video brightness profile provides an indirect measure of ice roughness, particularly if the pack ice is made up of ice rubble in water which provides dark/white variations in the images. The video brightness profiles give finer detail as the pixel size for these images is approximately 0.15 m, an order of magnitude smaller than the laser sample spacing.

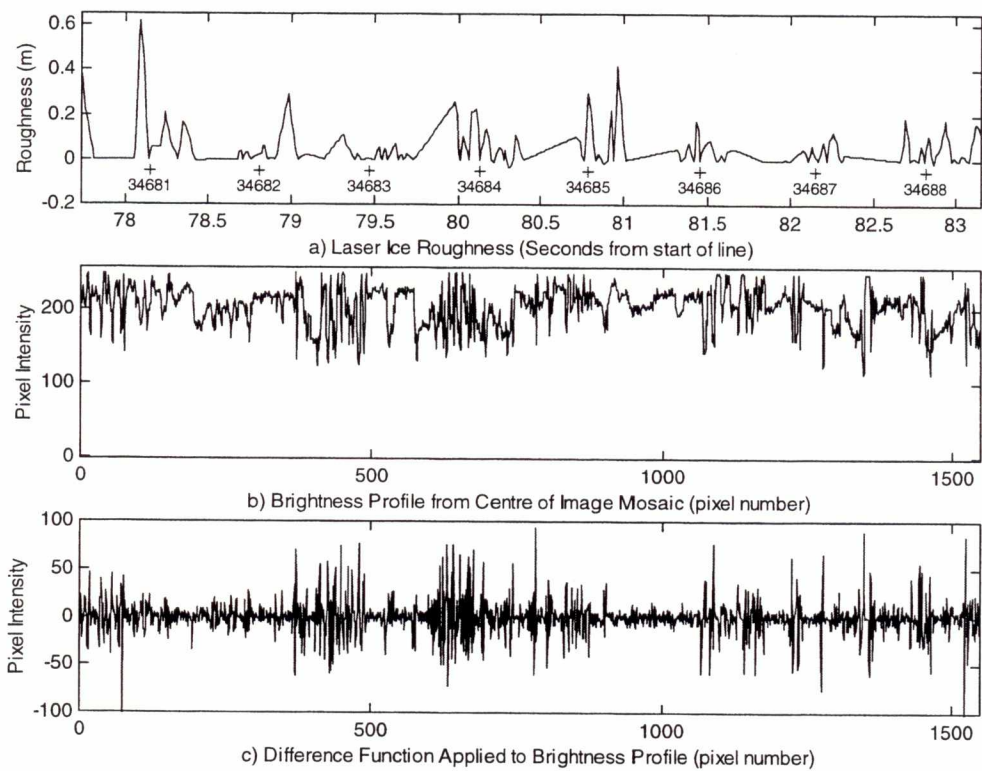


Figure 3.1.1 Laser roughness and image brightness profiles.

3.2 VIDEO MULTI-SPECTRAL ANALYSIS

This section explores the use of colour video imagery to extract additional information from the collected video data set. One use of colour information is to use the video data to classify the surface as either ice-covered or open water. Monochrome intensities of the video images do not lend themselves to this task as the video camera's variable iris varies the grey-scale intensities of the frames. For example thin ice may appear darker than open water in one frame and the other way around in the next.

The digital video images are stored as red, green and blue colour planes. Each colour plane is made up of 8 bit pixels for a range of intensities from 0 to 255. Images from March 1999 were used for this analysis since the 1999 image quality was far superior to the 1998 image quality (provided by a cabling change prior to the March 1999 field trial).

This analysis used a series of images from line 47 (D1999_060F047) collected on March 1, 1999. The image sequence runs from frame 27172 to 27661 for a total of 490 frames. The distance traversed along the flight line is approximately 14.9 km. The nominal frame capture interval is 0.5 seconds. The nominal flying height for this line was 50 m. From each image, a small section of 100 by 100 pixels was taken from the same location in each frame as shown in Figure 3.2.1.

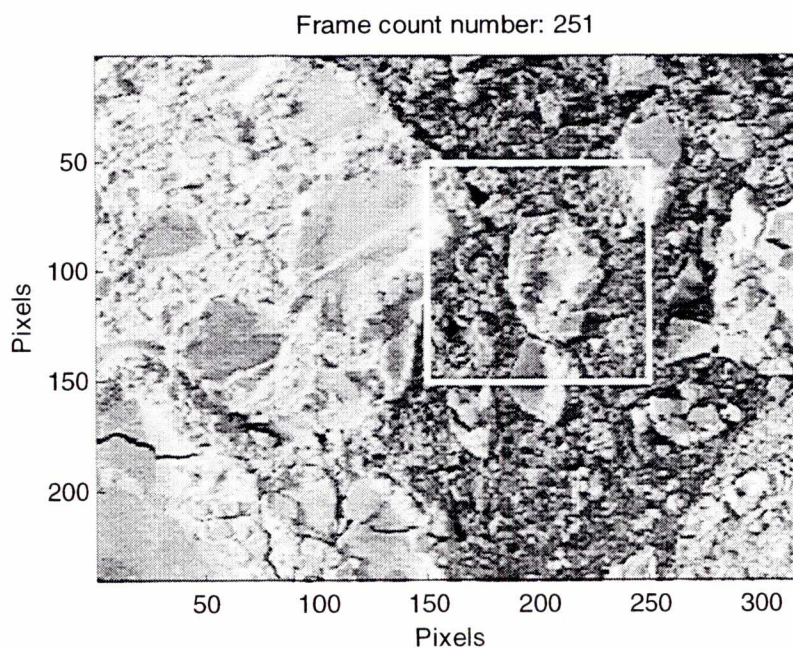


Figure 3.2.1 Plot of image count 251 from line 47 (flown on March 1, 1999) showing the area within the frame used for the colour analysis.

3.2.1 Manual Interpretation

The series of frames used are shown in Figure 3.3.1. A manual interpretation was performed to note the extent of the ice cover along the length of the profile. The manual interpretation is shown in Table 3.2.1. A visual scan through the images was made to roughly classify the ice cover. The letter codes shown in Table 3.2.1 do not correspond to a particular type of ice cover, they correspond to a change from previous conditions. Regions A, V and X are the only series of images where there is no ice at all. The last 80 frames (from frame count 411 on) are either over land or over land-fast ice.

3.2.2 Red-Green-Blue Analysis

For each video frame, the red, green and blue frames were handled separately. The mean pixel intensity was calculated for the small area for each colour plane in each frame. Figure 3.2.2 shows a plot of the mean intensity of each colour for the small area in each video frame in the sequence studied. Figure 3.2.3 shows a plot of the standard deviation of each colour for the small area in each video frame in the sequence studied. Annotations from Table 3.2.1 are added to the plots to indicate the surface conditions along the profile. The letters on the plot are centred within the frame count numbers provided in the table.

The plots for each colour follow each other very closely. Viewing colour information as individual red, green and blue image values does not provide any means of classifying the ice cover.

3.2.3 Hue-Saturation-Value Analysis

The method used to represent a stored colour image is called a *colour space*. The data logging system stores the images in a red-green-blue (RGB) colour space. The colour space for the series of images was converted to the Hue-Saturation-Value (HSV) colour space.

Value is the intensity of light seen. When a colour image is converted to grey-scale, the value parameter in the HSV colour space provides the grey-scale information directly (though the combination of colours to get grey-scale is not exactly the same as the standard grey scale conversion Y discussed below). Hue is the attribute of colour that is defined by the dominant wavelength of light. Saturation is the attribute of colour that defines the degree of colour vividness. With high saturation levels, the colours are bright, with low saturation levels the color are pastel-like. Saturation levels of zero are a shade of grey where the grey shade is determined by the value level.

With HSV color space, a Hue of 0 degrees is red, 60 is yellow, 120 is green, 180 is cyan, 240 is blue and 300 degrees is magenta. Saturation and Value range from 0 to 255. The units are normalized in the figures.

The mean pixel intensity was calculated for the small area for each HSV plane in each frame. Figure 3.2.4 shows a plot of the mean levels of each colour for each of the HSV planes for each video frame in the sequence studied. Figure 3.2.5 shows a plot of the standard deviation of the HSV planes for each video frame in the sequence studied. Annotations from Table 3.2.1 are added to the plots to indicate the surface conditions along the profile.

In Figure 3.2.4 the mean hue value is remarkably smooth. In the areas of ice cover, the hue value is high, in areas of open water (A, V and X) the values are low.

3.2.4 NTSC Colour Space (YIQ) Analysis

Another colour space was looked at. The NTSC (National Television System Committee) colour space transformation (Fink and Christiansen, 1982) has a grey scale plane (Y) like V in the HSV space and two chrominance planes (I and Q). The chrominance planes are made from combinations of red, blue and Y colour planes. Figure 3.2.6 shows a plot of the mean levels of each colour for each of the NTSC planes for each video frame in the sequence studied. Figure 3.2.7 shows a plot of the standard deviation of the NTSC planes for each video frame in the sequence studied. The units have been normalized.

In Figure 3.2.6 the mean Q value is remarkably smooth at the beginning area of open water (zone A) and the level is low. At the other areas of open water (V and X) the Q levels are also low.

Table 3.2.1 Manual interpretation of surface ice features for line 47 (D1999_060F047) collected on March 1, 1999.

Region	Frame #	Frame count	Surface conditions
A	27173-27225	2 – 54	Open water, very few small floes
B	27226-27235	55-64	Full coverage of slush with a few small floes
C	27236-27238	65-67	Large floe
D	27239-27242	68-71	Young ice recently broken up
E	27243-27246	72-75	Young ice
F	27247-27255	76-84	Slush rubble with a few medium floes
G	27256-27265	85-94	Slushy rubble with sm. and lrg floe + area of open water
H	27266-27271	95-100	Large floe
I	27272	101	Open water, small and med floes
J	27273-27278	102-107	Slushy rubble with large floe
K	27279-27281	108-110	Large floe
L	27282-27293	111-122	Recently brkn lrg floe with some slushy rubble
M	27294	123	Open lead between large floes
N	27295-27312	124-141	Sm, med and lrg floes w slushy rbl and ridging
O	27313-27322	142-151	Large and med floes with 10% open water
P	27323-27325	152-154	Large floe
Q	27326-27342	155-171	Med and large floes with some slushy rubble
R	27343-27345	172-174	Small floes with slushy rubble
S	27346-27352	175-181	Recently broken floe with some open water
T	27353-27445	182-274	Sm, med and large floes with slushy rubble
U	27446-27466	275-295	Sm, med and large floes w slushy rubble + some open water
V	27467-27472	296-301	Open water
W	27473-27490	302-319	Sm, med floes sep by open water (473-482 used in floe size meas.)
X	27491-27503	320-332	Open water
Y	27504-27508	333-337	Dense small floes surrounded by slushy rubble
Z	27509-27511	338-340	Large floe with leads
AA	27512-27520	341-349	Large floe
BB	27521-27524	350-353	Med and large floes w some open water
CC	27525-27527	354-356	Sm floes sur. by slushy rbe + some open water
DD	27528-27553	357-382	Med and large floes w slushy rubble + no open water
EE	27554-27557	383-386	Med + lrg floes w slushy rbl + some opn water
FF	27558-27569	387-398	Young ice with some recent breakup and small amount of open water
GG	27570-27581	399-410	Young ice with a few open leads
HH	27582-27619	411-448	Over land
II	27620-27651	449-480	Land fast ice
JJ	27652-27661	481-490	Shoreline

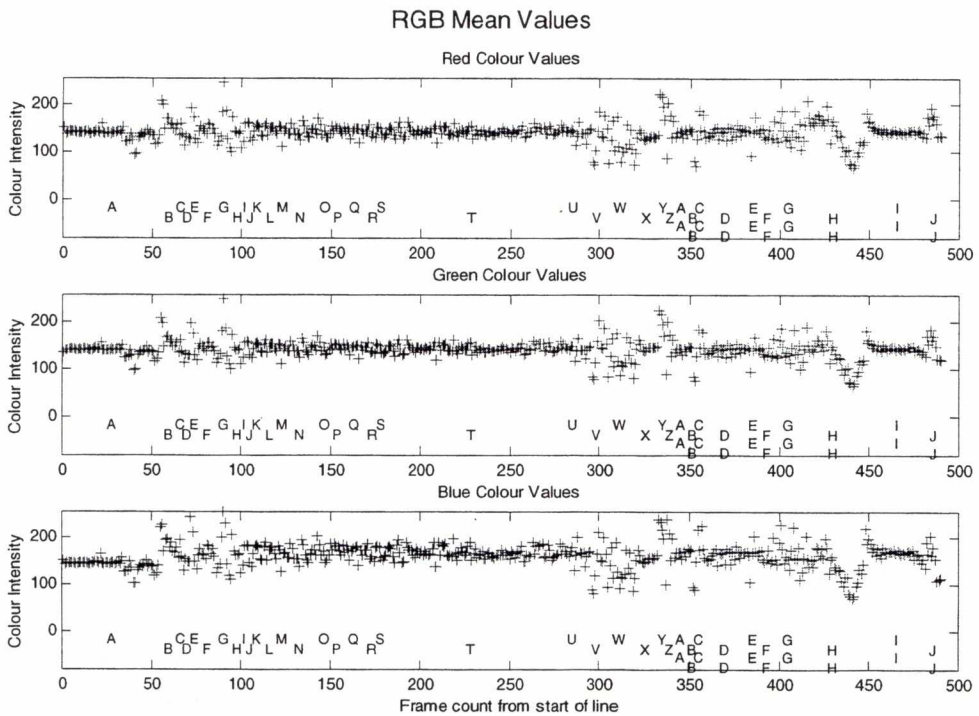


Figure 3.2.2 Plot of RGB mean values along line 47 (averaged over a small area of image).

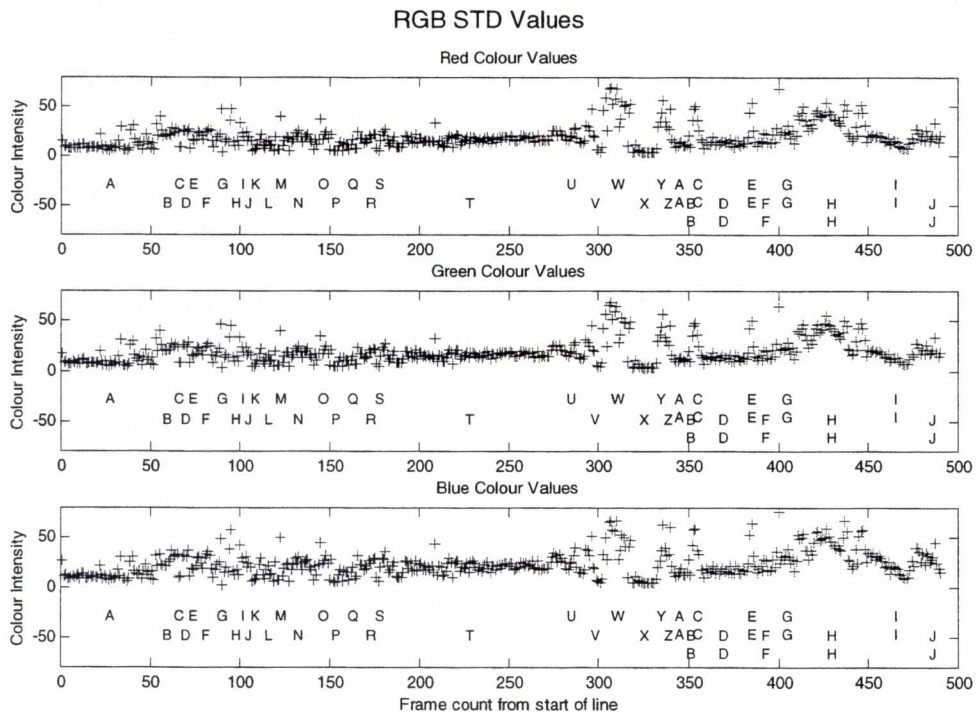


Figure 3.2.3 Plot of RGB standard deviation (STD) values along line 47 (averaged over a small area of image).

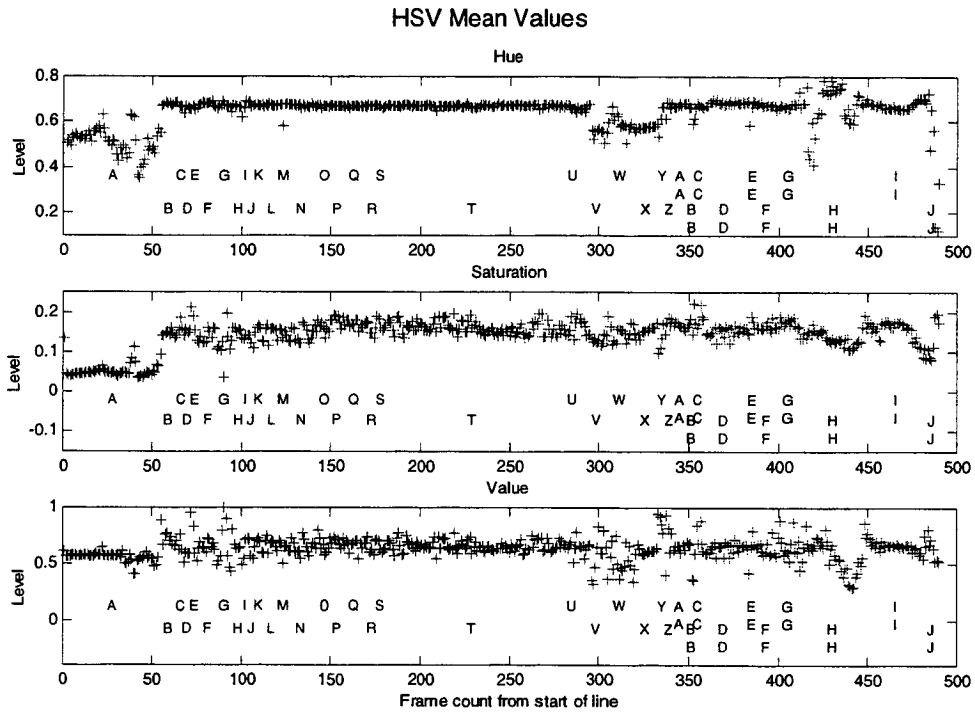


Figure 3.2.4 Plot of HSV mean values along line 47 (averaged over a small area of image).

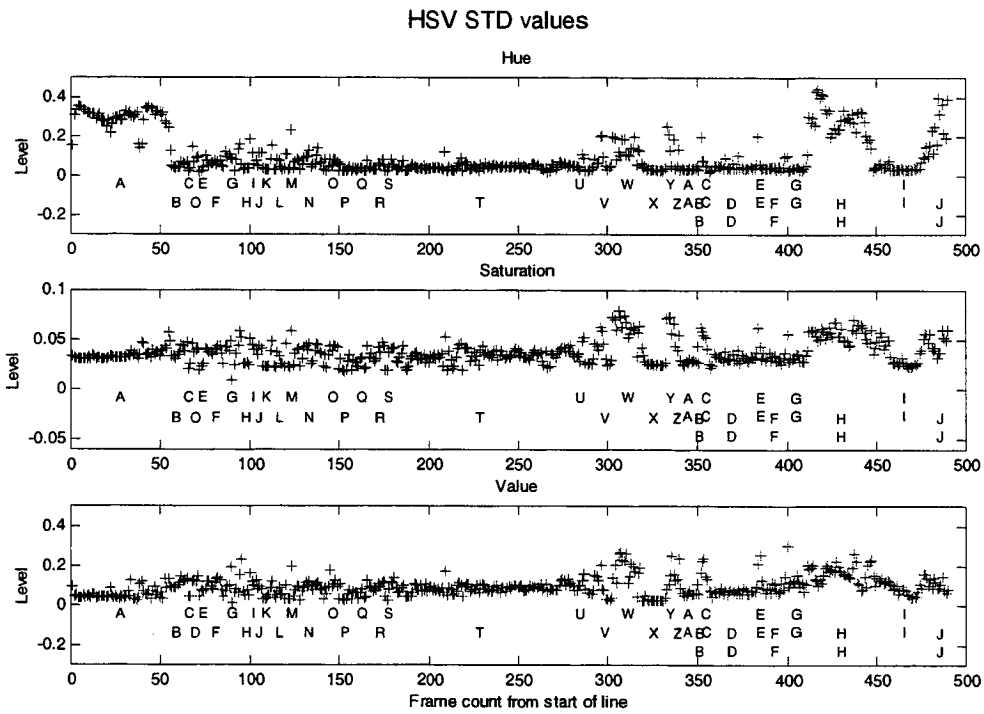


Figure 3.2.5 Plot of HSV standard deviation (STD) values along line 47 (averaged over a small area of image).

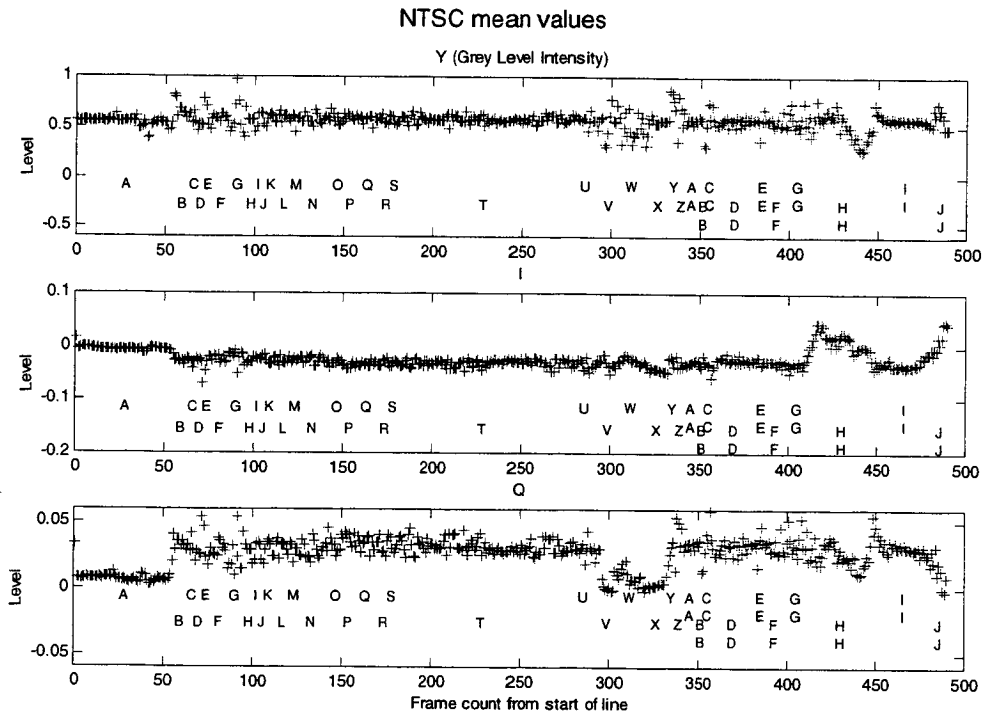


Figure 3.2.6 Plot of NTSC YIQ mean values along line 47 (averaged over a small area of image).

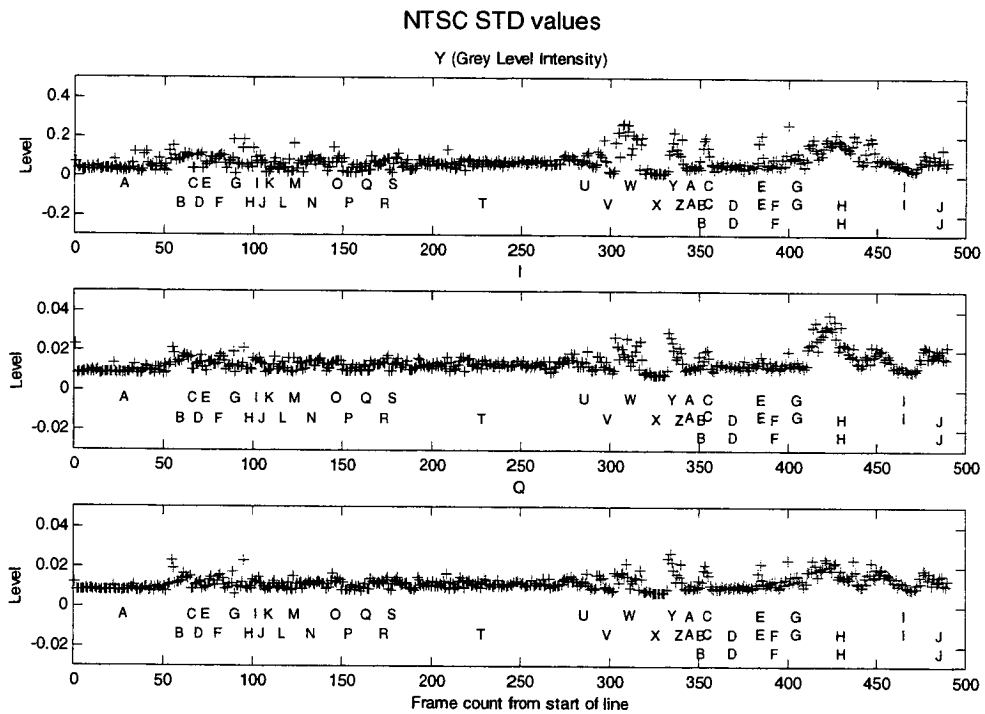


Figure 3.2.7 Plot of NTSC YIQ standard deviation (STD) values along line 47 (averaged over a small area of image).

3.3 VIDEO IMAGE PLOTTING

The digital video collected by the system is a very large volume of data that has been difficult to work with. Previously there were two ways to view the video data, either by looking at individual frames, or by converting a series of images into an AVI file format which can be played back as a movie on a computer's video display. To scan through a data set for visual analysis or to archive or distribute results an efficient presentation method is required. Two techniques were looked at, a quick-look plot and geo-referenced images plotted alone or with a map base.

3.3.1 Quick Look Plots

Quick-look plots can be used to scan the full survey's imagery with a plot that provides the maximum amount of imagery on a single page. These plots are quick to produce since very little manipulation of the image data is performed. Prototype Matlab routines have been developed to demonstrate this presentation technique.

Figure 3.3.1 shows a quick-look plot for a line flown at a nominal altitude of 50 m. These images are from line 47 (D1999_060F047) collected on March 1, 1999. The image sequence runs from frame 27172 to 27661 for a total of 490 frames. The distance traversed along the flight line is approximately 14.9 km. The average frame capture interval is 0.5 seconds. For this plot the pixel size is assumed to be 0.25 m.

The quick-look plots provide an image sequence that starts at the top left corner of a page with subsequent frames plotted towards the right (overlapping each other) following the survey helicopter's along-track distance traveled. Subsequent rows plotted under each other permit plotting of an entire survey line. GPS positioning data is processed to provide frame-to-frame image separation in metres. The average flying height for the survey line is used to determine the size of the image pixels in metres at the surface. The plot will appear distorted if there is any variation in helicopter motion. Best results will be obtained when the helicopter is flying straight without any cross winds that would cause the helicopter to crab. An example of crabbing can be seen in Figure 3.3.1 where the image series from 427 to 440 shows the shoreline.

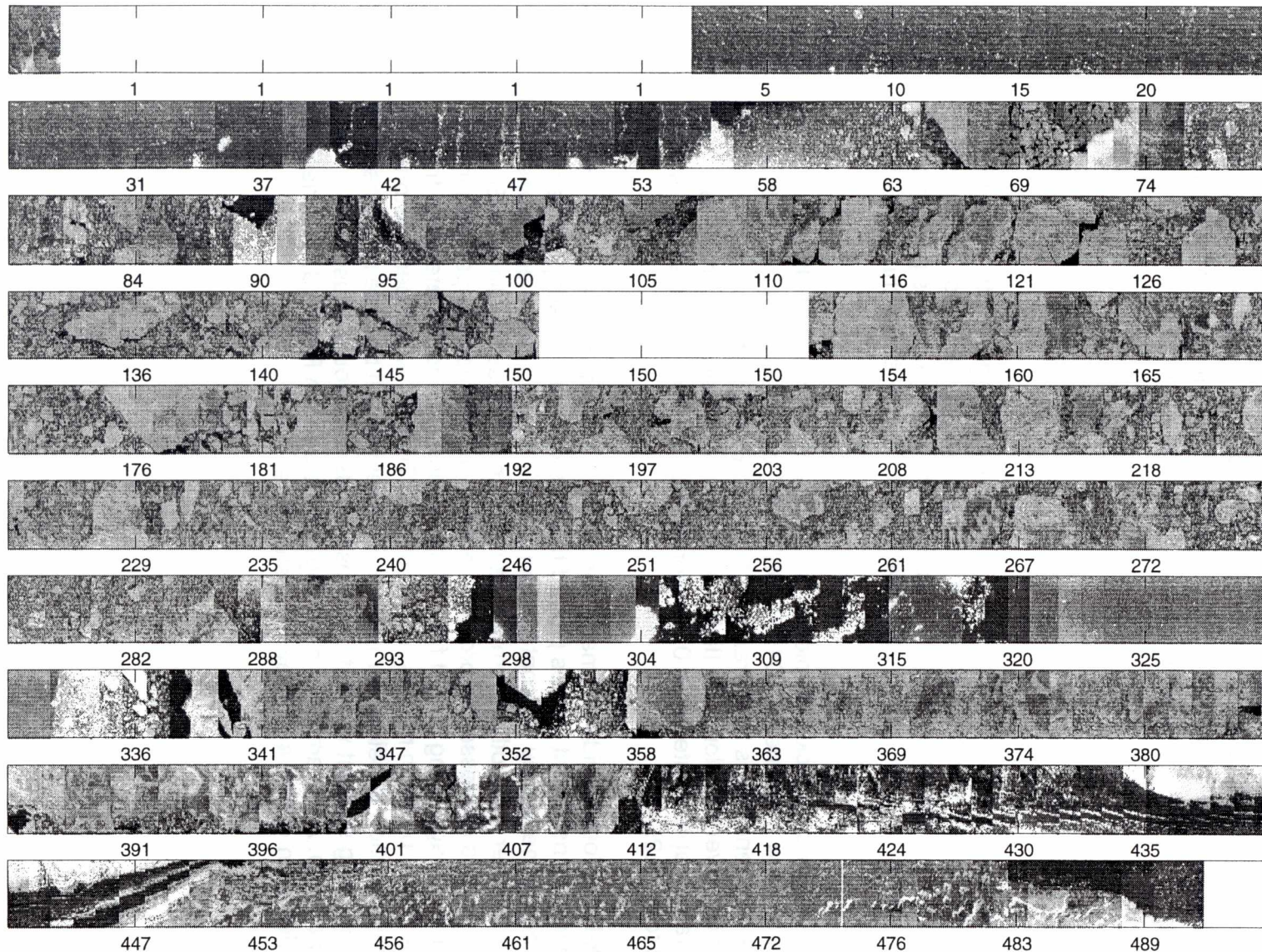


Figure 3.3.1 Quick-look plot for line 47 (D1999_060F047) collected on March 1, 1999 at a nominal altitude of 50 m. The line length is approximately 14.9 km.

Several long sections of the plot show uniform image brightness, for example from frame number 197 to frame 282. Other areas show large brightness changes from frame to frame, examples can be seen at frames numbers 90, 95 298 and 352. The change in brightness is due to the camera's auto-iris adjustments changing due to the changing scene. If there is mostly open water, then the ice will be appear completely white with no detail. If there is only ice then the ice appears grey and details in the ice can be seen. A change in the image brightness may provide an indication that the surface ice characteristics have changed. Also, brightness changes may be due to changes in cloud cover.

The plotting routine can be adjusted to show more or less detail on a page and have the plot continue over multiple pages. Prints can be made on 11" by 17" paper for greater detail or coverage. The full image width is plotted so the detail of the final plot is determined by the hard copy medium of the file format used to store the figure (for importing into a word processor).

3.3.2 Geo-referenced Image Plots

The geo-referenced image plots use GPS latitude, longitude and heading information to make a plot. The latitude and longitude positions are converted to UTM-based metre coordinates so that the images can be plotted to a map scale.

The heading information is used to orient the images on the plot. As a result, the images do not align perfectly, but geographic positioning of visual ice features aids with the data analysis.

Figure 3.3.2 shows a geo-referenced image plot from a flight flown at an altitude of 50 m. This plot uses a subset of the images approximately 2.8 km long (frame numbers 251 to 350) from line 47 (D1999_060F047) collected on March 1, 1999.

Figure 3.3.3 shows a geo-referenced image plot from a flight flown at an altitude of 300 m. This flight line was flown over the Confederation Bridge and is approximately 13.5 km long. This plot uses all the images (a total of 114 frames) from line 49 (D1999_060F049) collected on March 1, 1999.

A map base can be added to the geo-referenced image plots as shown in Figure 3.3.4. This plot uses all the images (a total of 98 frames) from line 86 (D073F086) collected on March 14, 1998. This line was flown at an approximate altitude of 2500 m and is approximately 50 km long. This altitude is beyond the range of the laser or radar altimeters. During the flight the helicopter's barometric altimeter readings were logged in a notebook.

The plotting of single profile lines is very inefficient using this technique compared with the quick-look plot shown in Figure 3.3.1. The individual frames are smaller in the geo-reference plot and fewer frames are plotted per printed

page. A combination plot using a flight path track plot and the quick look plot may be best for operational use.

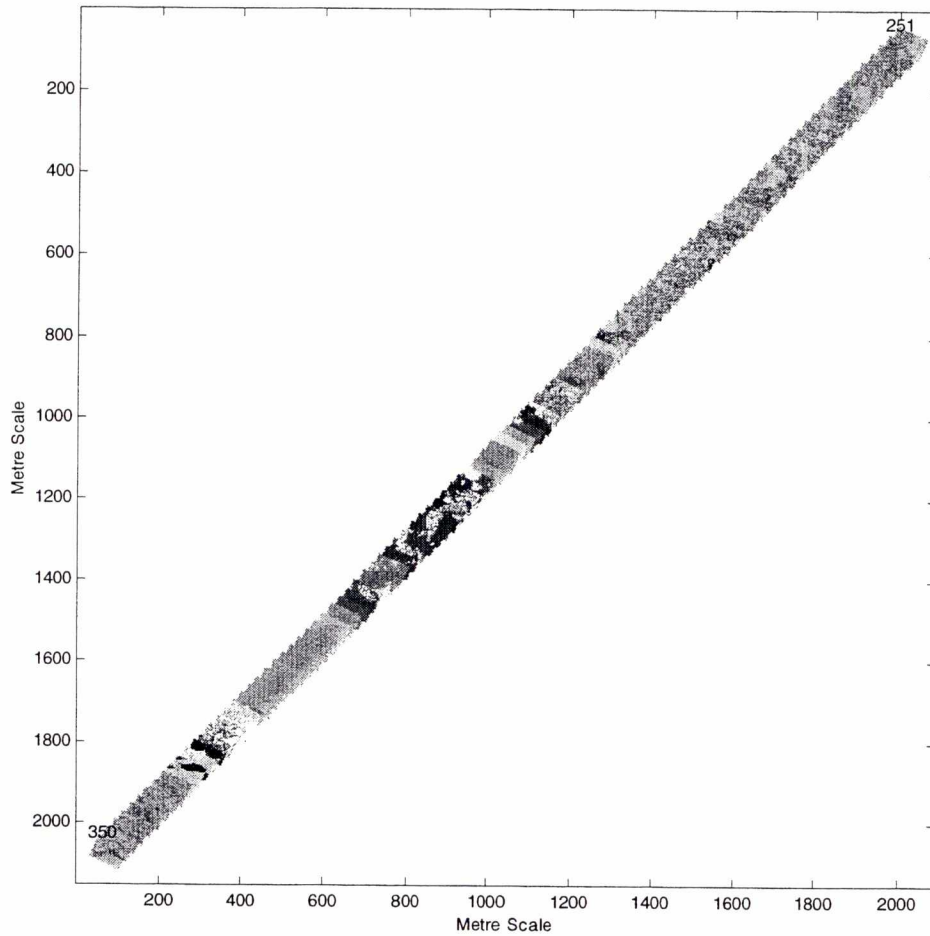


Figure 3.3.2 Geo-referenced plot for line 47 (D1999_060F047) collected on March 1, 1999 at a nominal altitude of 50 m.

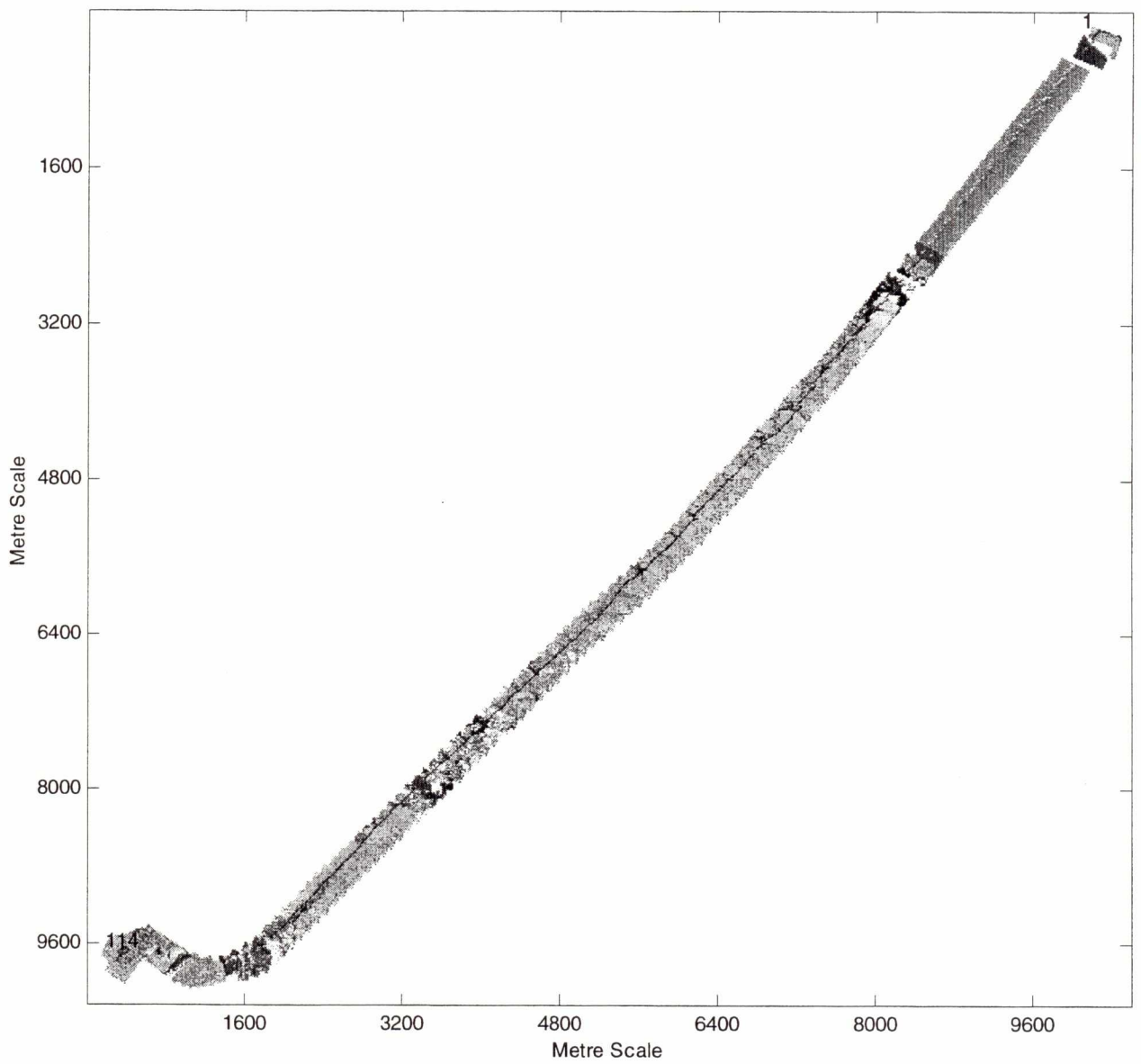


Figure 3.3.3 Geo-referenced plot for line 49 (D1999_060F049) collected on March 1, 1999 at a nominal altitude of 300 m.

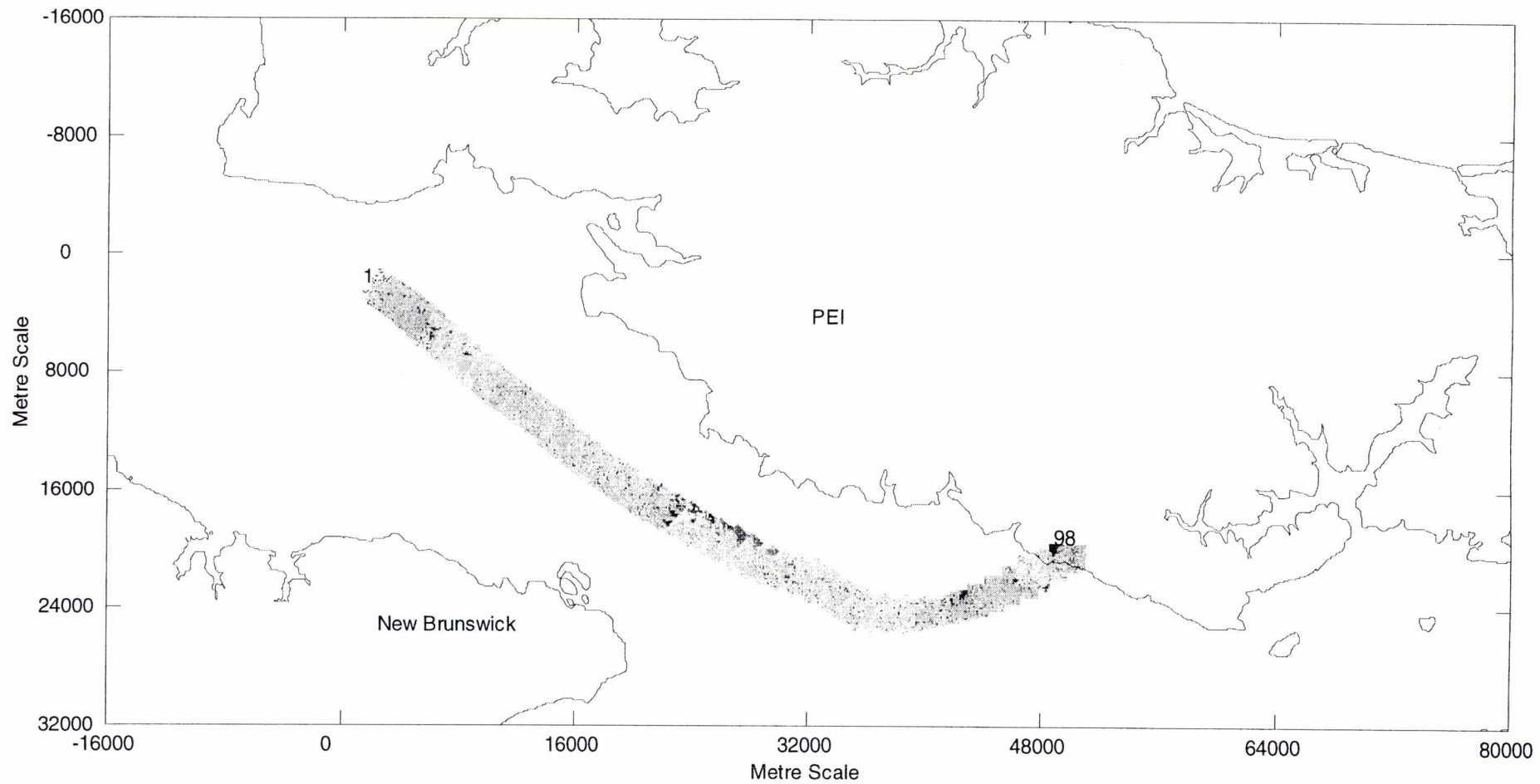


Figure 3.3.4 Geo-referenced plot with a map base for line 86 (D073F086) collected on March 14, 1998 at a nominal altitude of 2500 m.

4 ICE PARAMETER MEASUREMENT

4.1 ICE FLOE SIZE MEASUREMENT

Ice floe sizes can be measured manually, but the measurements are very labour-intensive and due to the large number of video frames collected manual measurements of floe size are not practical. A review of image processing techniques available was made to determine if an automated floe measurement procedure could be assembled. After searching the Internet and reviewing Matlab manuals a preliminary automatic floe size measurement routine was assembled. The automatic processing routine was performed on a series of ten images. For comparison purposes, manual floe size measurements were made over the same series of images. The results are discussed below.

The images used for the floe size measurements are taken from line 47 (D1999_060F047) collected on March 1, 1999. The flight was flown at a nominal altitude of 50 m. Ten images starting from frame number i0027475 were used as the floes are generally small and well separated. Counting from the start of the survey line, the images are numbered from 1 to 490. They can be seen in the quick-look plot shown in Figure 3.3.1. Figure 4.1.1 shows a plot of the ten unprocessed images in grey-scale form.

4.1.1 Manual technique

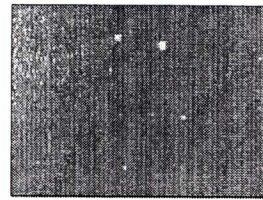
Manual floe size measurements required the following steps:

- Load image into Matlab
- Convert image to grey scale and plot
- Use mouse to click around perimeter of all floes in image
- Convert floe perimeters into pixel area
- Scale pixel area to surface area in square metres
- Create floe size histograms.

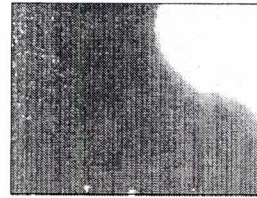
A graphical user interface was written to handle this task. Figure 4.1.2 shows the Matlab window which provided the functionality required to manually digitize the ice floes.

Figure 4.1.3 shows the ten images with an overlay of the manually digitized floe outlines. Figure 4.1.4 a) to j) show histogram plots of floe size for each of the ten images.

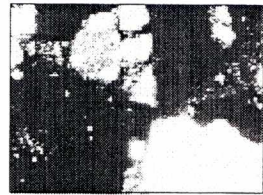
Original images in grey-scale



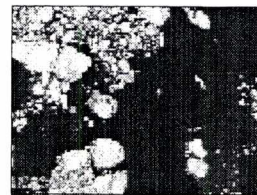
i0027473.bmp



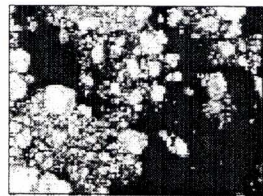
i0027474.bmp



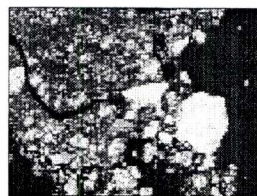
i0027475.bmp



i0027476.bmp



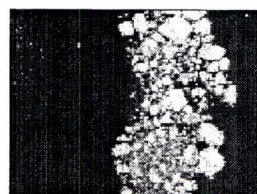
i0027477.bmp



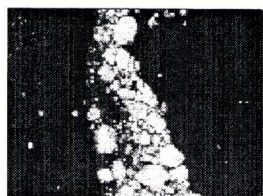
i0027478.bmp



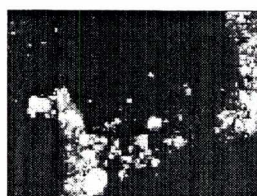
i0027479.bmp



i0027480.bmp



i0027481.bmp



i0027482.bmp

Figure 4.1.1 Plot of the original grey-scale images used for the floe size measurements

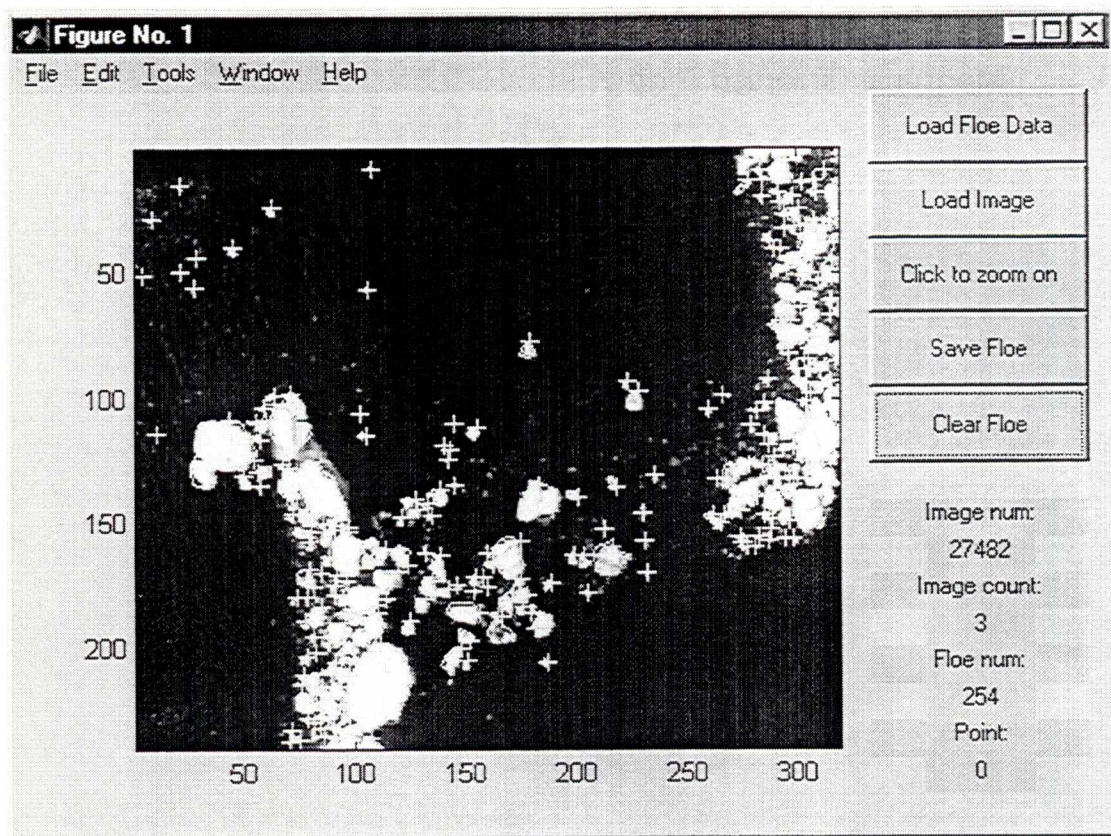


Figure 4.1.2 Matlab graphical user interface developed for manual floe size measurements.

Manually Outlined Floes

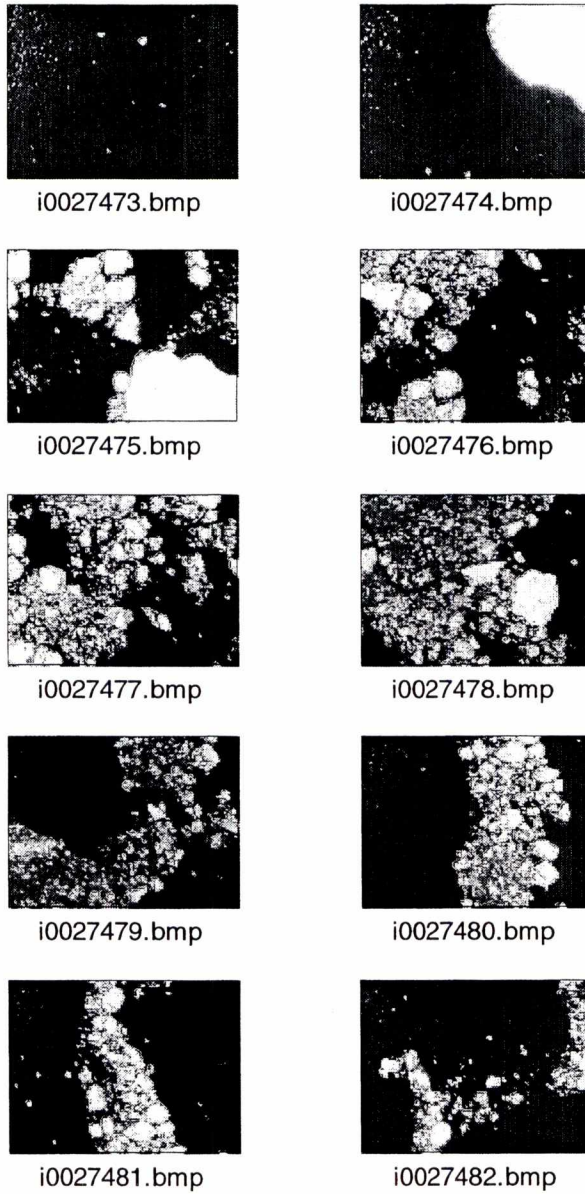


Figure 4.1.3 Plot of 10 images with an overlay of the manually-digitized floe outlines.

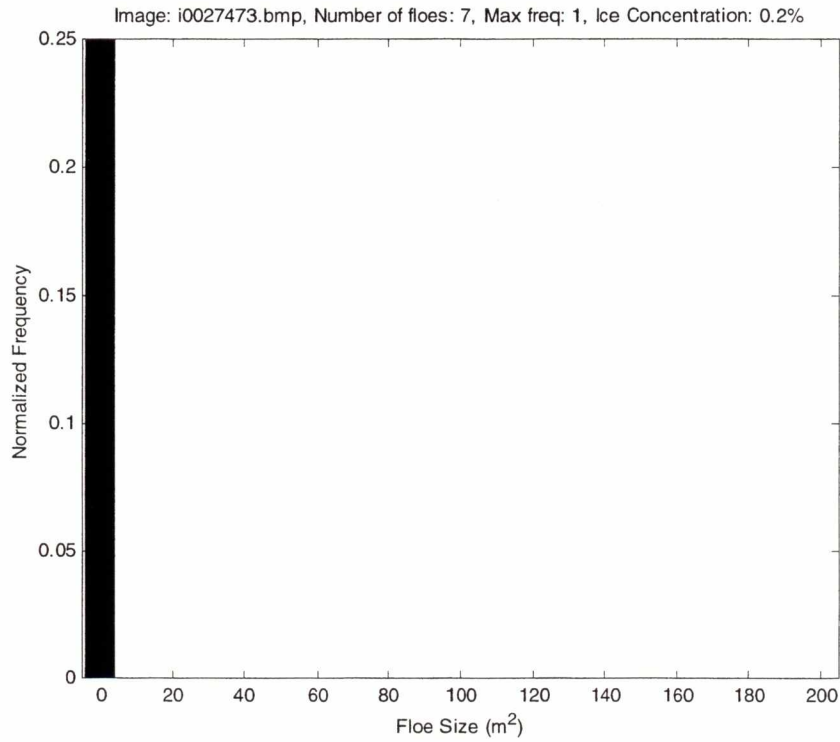


Figure 4.1.4 a) Histogram of floe size.

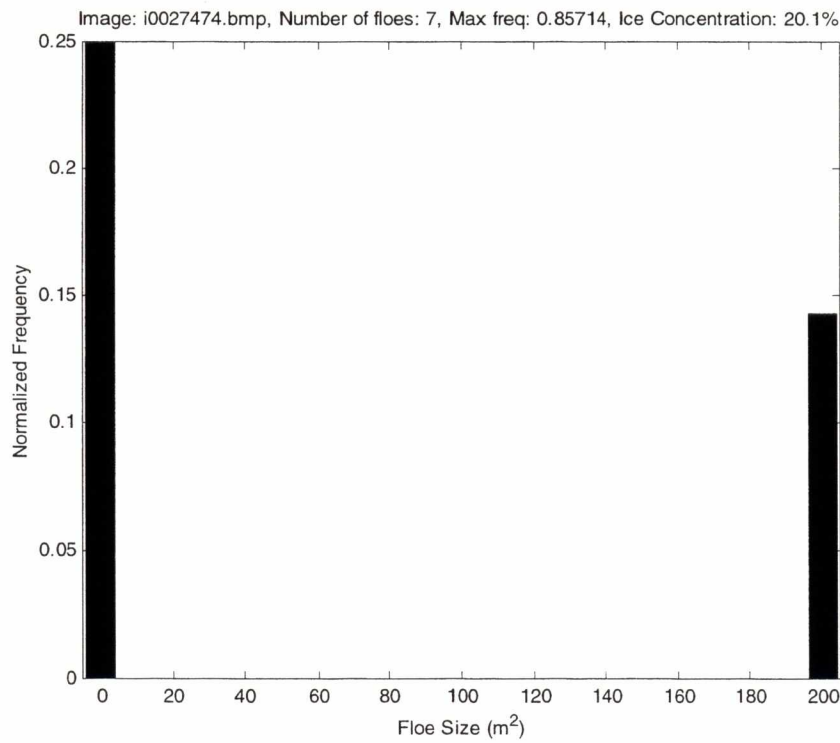


Figure 4.1.4 b) Histogram of floe size.

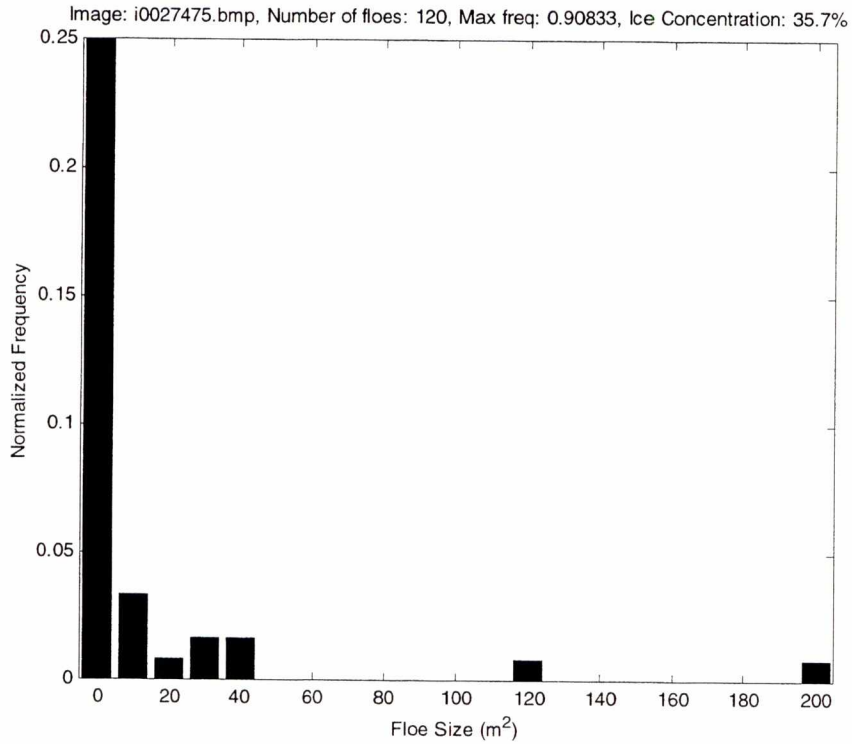


Figure 4.1.4 c) Histogram of floe size.

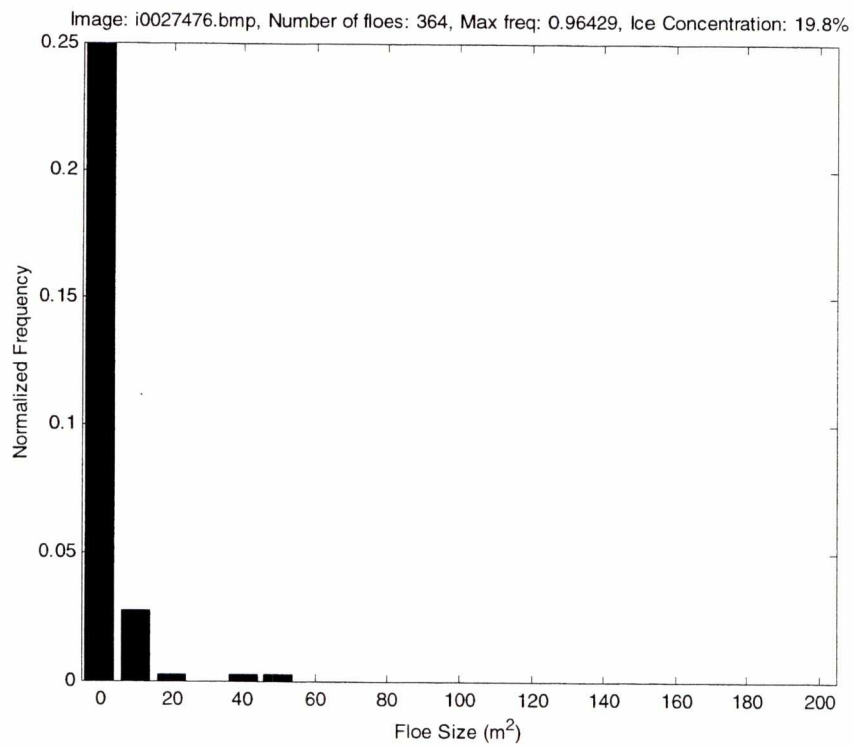


Figure 4.1.4 d) Histogram of floe size.

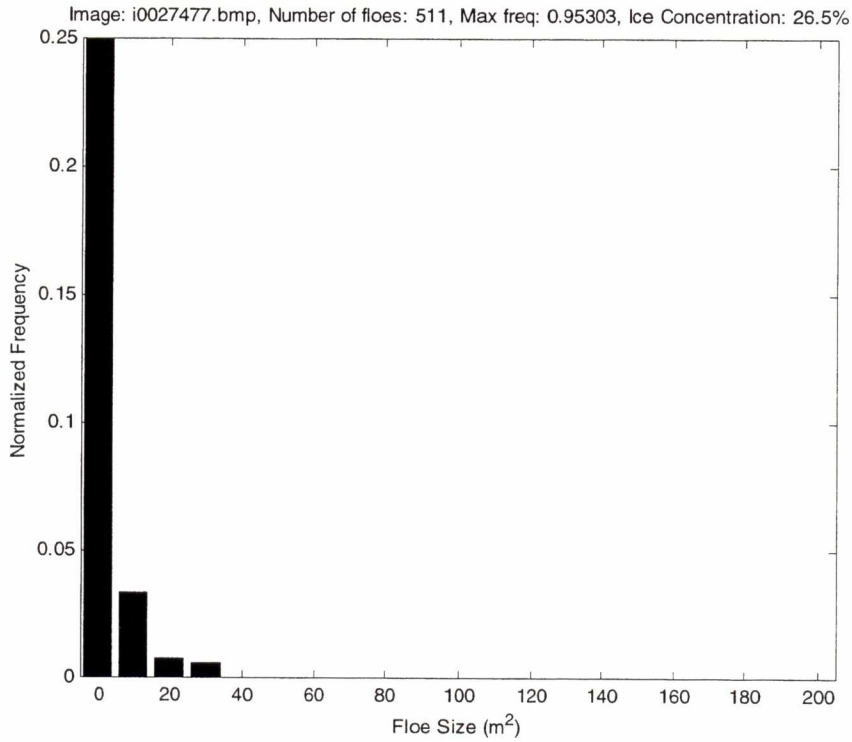


Figure 4.1.4 e) Histogram of floe size.

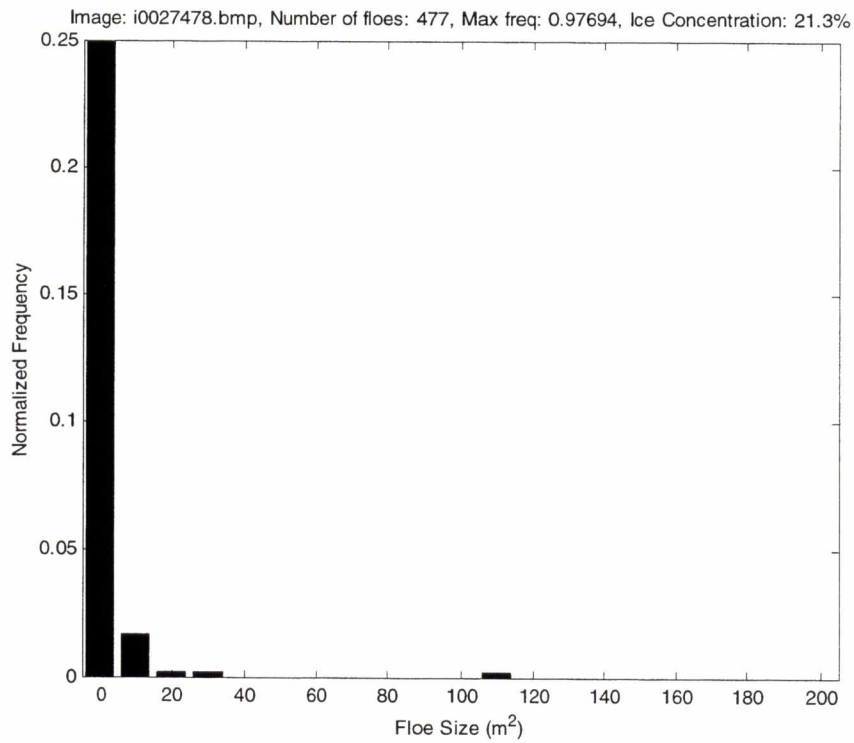


Figure 4.1.4 f) Histogram of floe size.

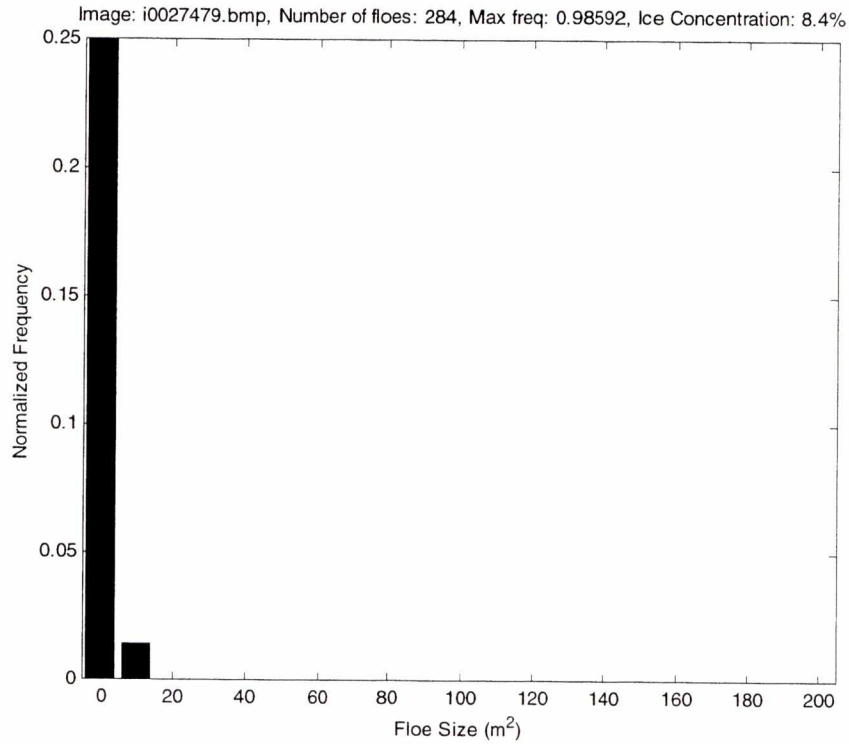


Figure 4.1.4 g) Histogram of floe size.

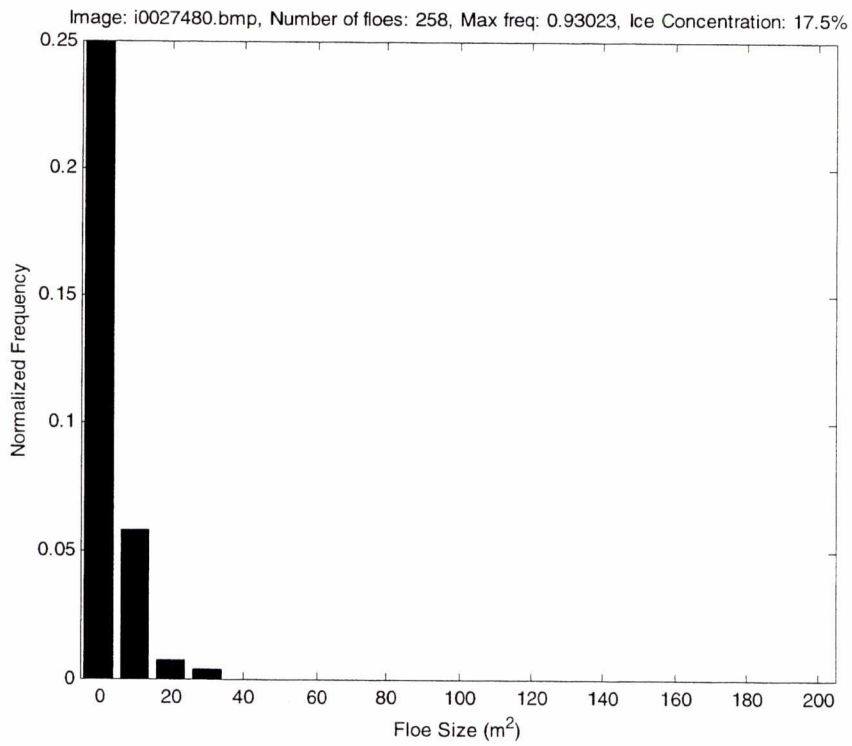


Figure 4.1.4 h) Histogram of floe size.

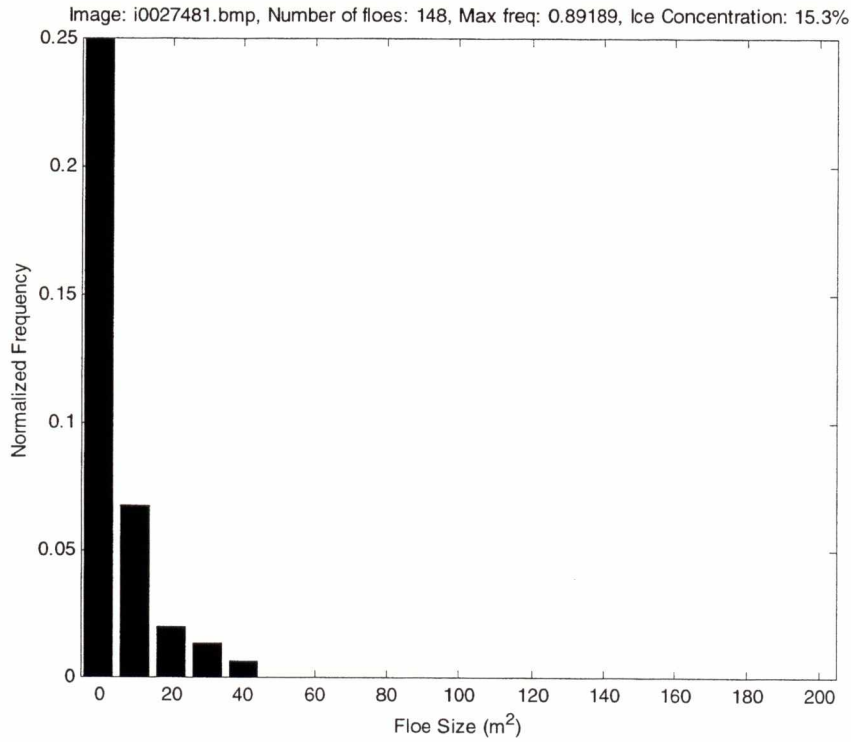


Figure 4.1.4 i) Histogram of floe size.

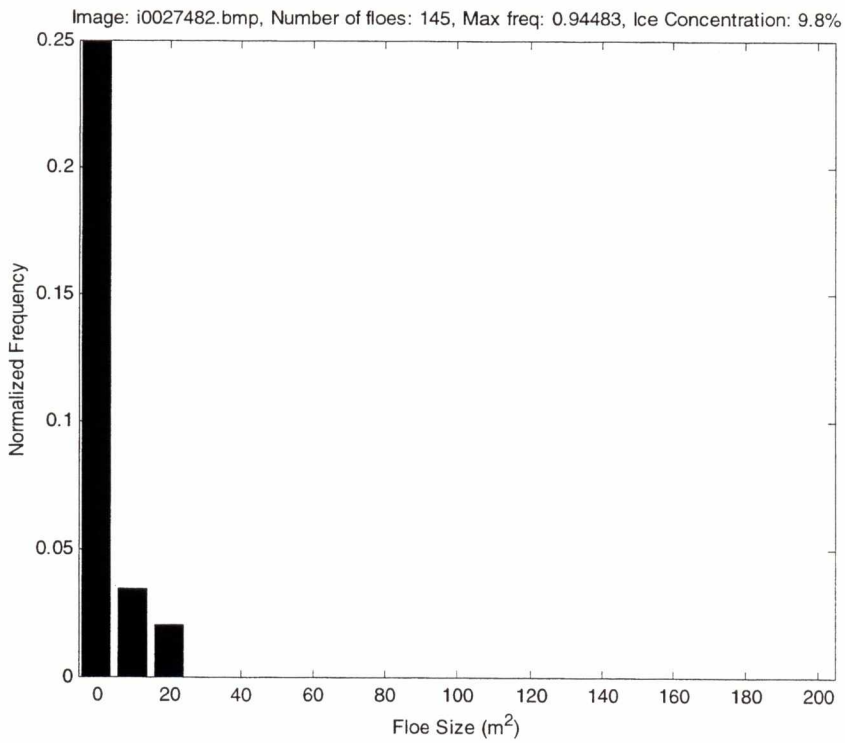


Figure 4.1.4 j) Histogram of floe size

4.1.2 Automatic Technique

The automated floe size measurement technique is based upon connected components analysis (Haralick and Shapiro, 1992). The processing steps are:

- Load image into Matlab
- Convert image to grey scale
- Apply a binary threshold.
- Apply connected components analysis to preprocessed image
- Count up the number of pixels in each identified floe to get pixel area
- Scale pixel area to surface area in square metres
- Create floe size histograms.

The binary thresholding assigns all pixels with intensity greater than or equal to the threshold value to one to represent ice. All pixels less than the threshold are assigned to zero to represent open water.

Connected components analysis scans through the binary-thresholded image to find the first pixel equal to one. This pixel is tagged with a floe number. If a pixel immediately above, below, left or right is also one then that pixel is also tagged with the floe number. The search continues with each tagged adjacent pixel until there are no longer any adjacent pixels with the value of one. The floe count is incremented and the next non-zero pixel is located to continue the procedure.

Figure 4.1.5 shows the ten images with the floes detected by the connected components analysis shown as various shades of grey (to distinguish each detected floe). Figure 4.1.6 a) to j) show histogram plots of automatic ice floe size for each of the ten images.

4.1.3 Discussion

Successful separation of ice and open water in the preprocessing steps (steps before the connected component analysis) is critical for good identification of individual floes. For this example, the only adjustable parameter was the binary threshold level. The search in the connected components analysis does not include pixels that are diagonally adjacent such as above-right or below-left. Including those pixels would reduce the technique's ability to separate adjacent floes from one another. To support a wider variety of image types, further trials with various morphological image processing techniques are required to provide increased separation between adjacent floes.

Connected Components Images

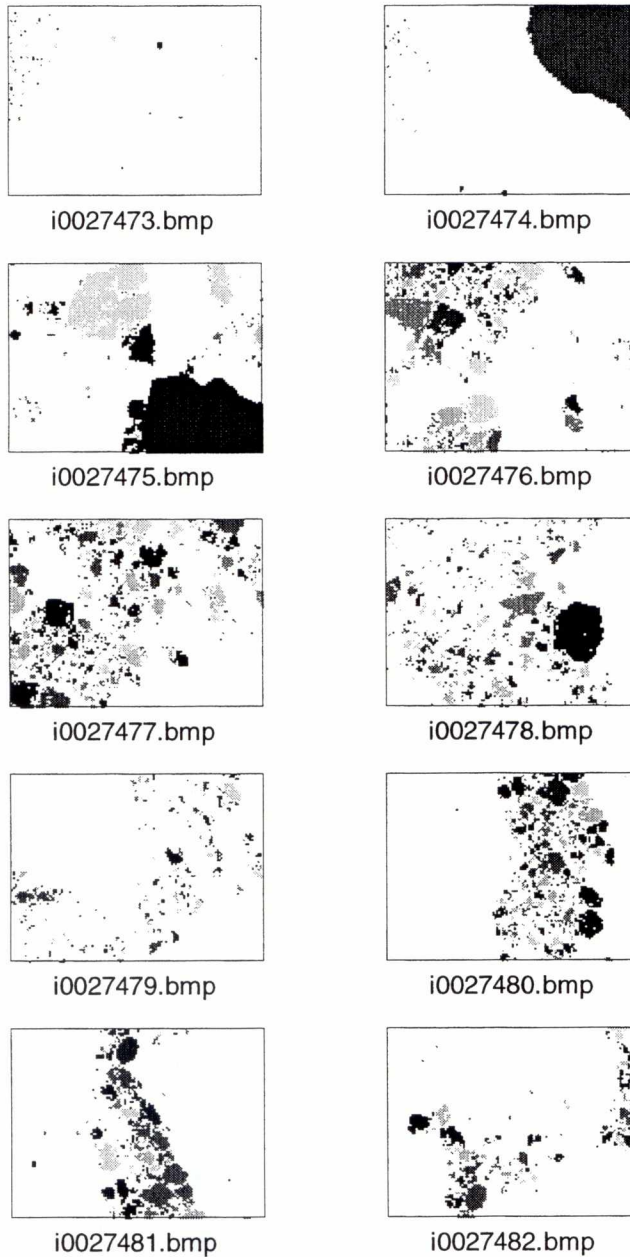


Figure 4.1.5 Plot of 10 images with a grey-scale coding to indicated the floes identified by the connected components analysis for the automatic floe size processing routine.

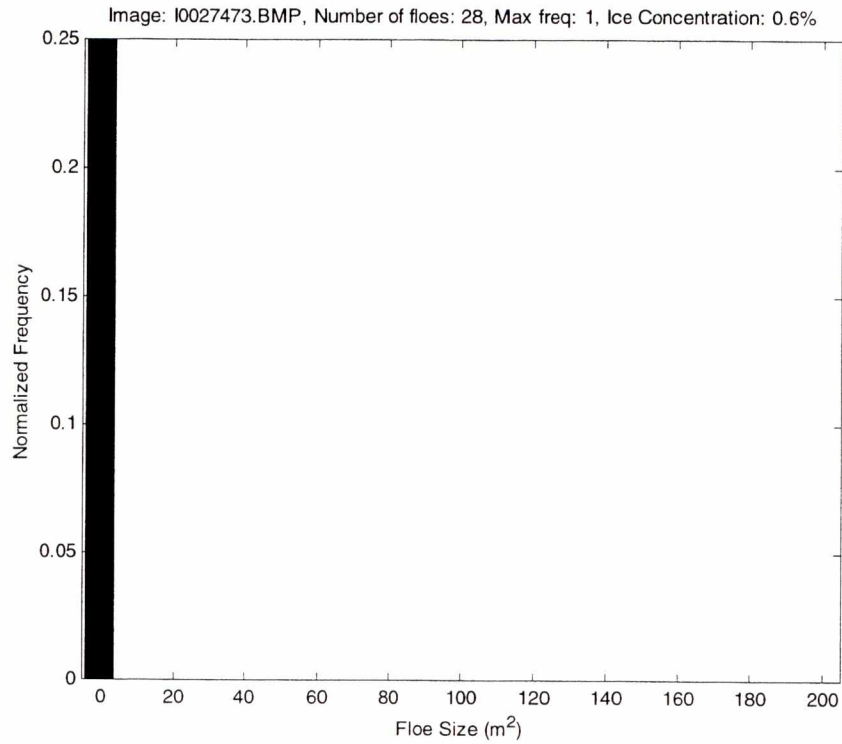


Figure 4.1.6 a) Histogram of floe size.

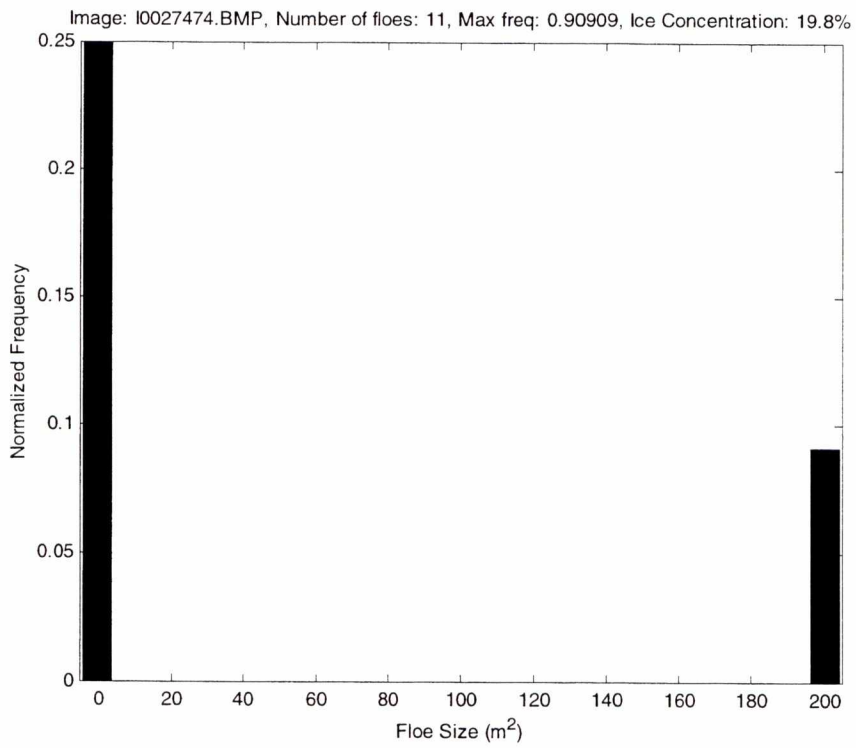


Figure 4.1.6b) Histogram of floe size.

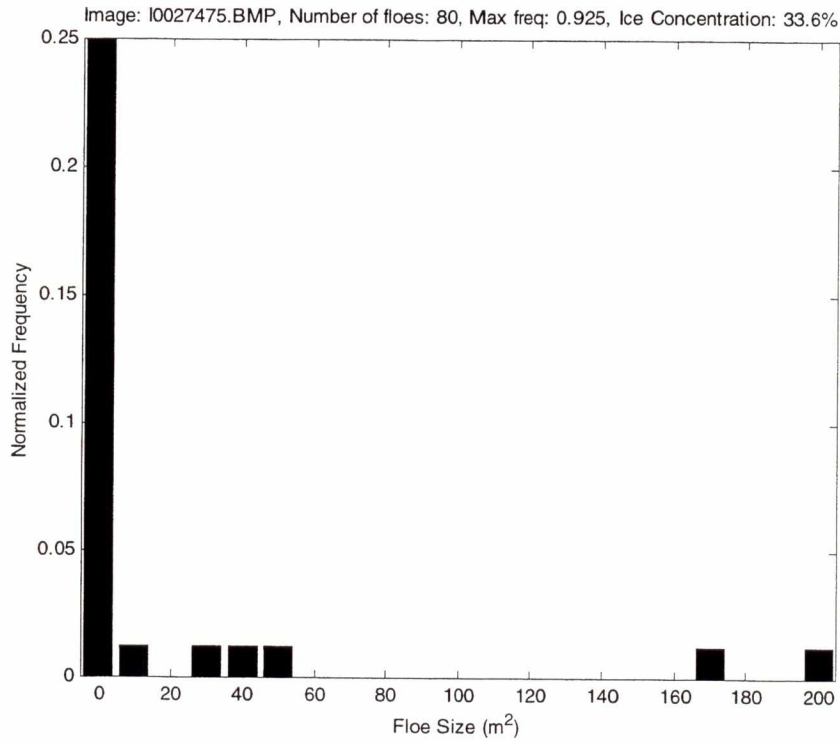


Figure 4.1.6 c) Histogram of floe size.

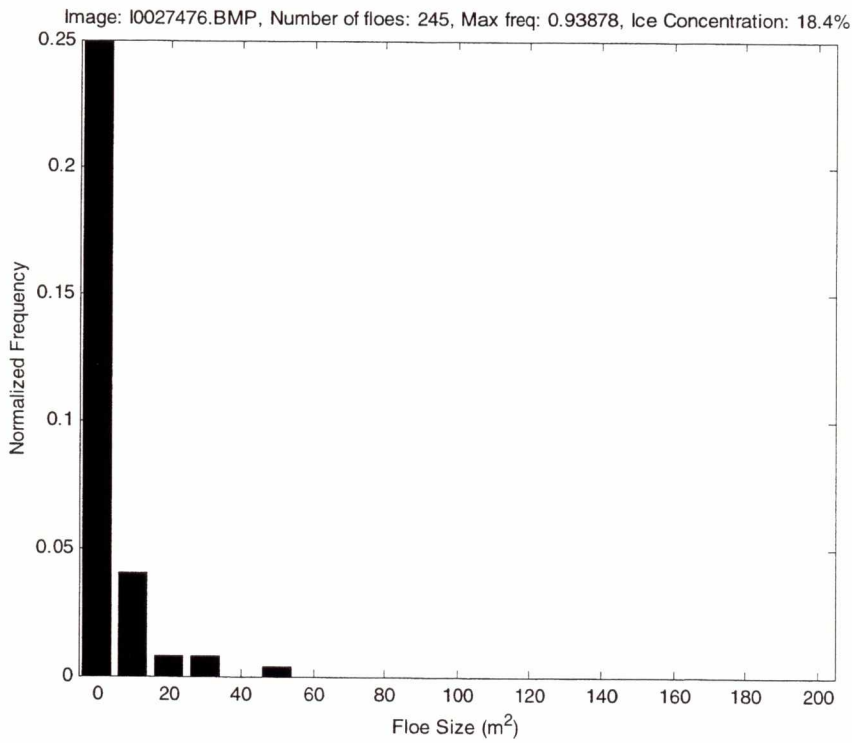


Figure 4.1.6d) Histogram of floe size.

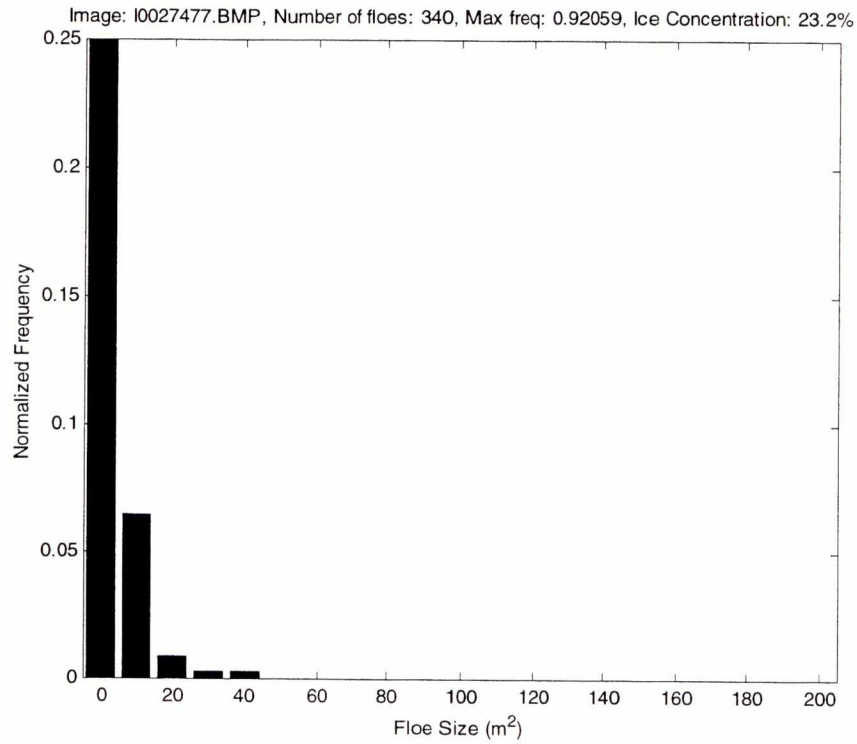


Figure 4.1.6e) Histogram of floe size.

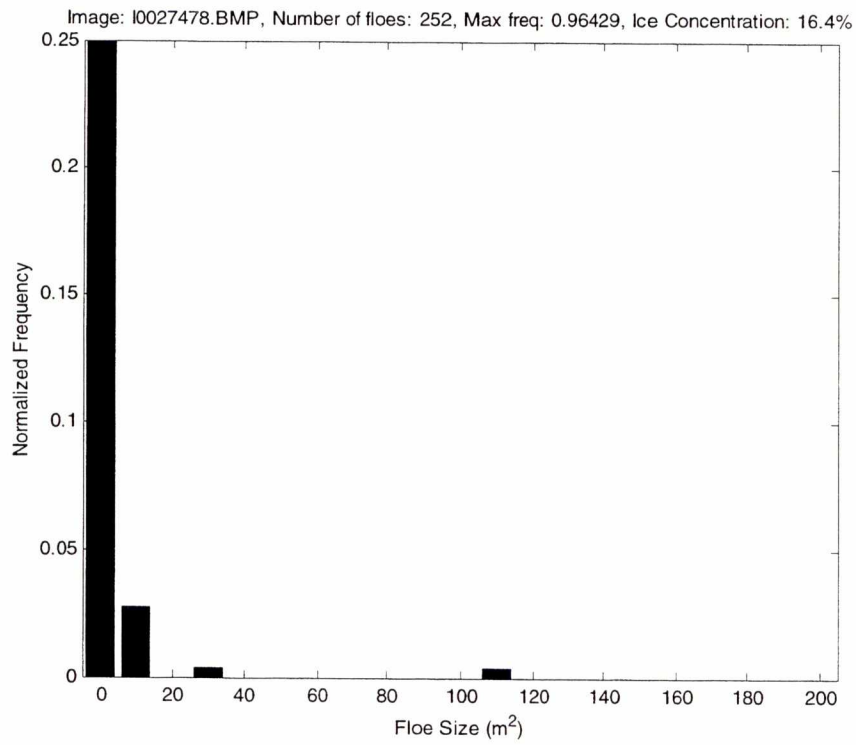


Figure 4.1.6f) Histogram of floe size.

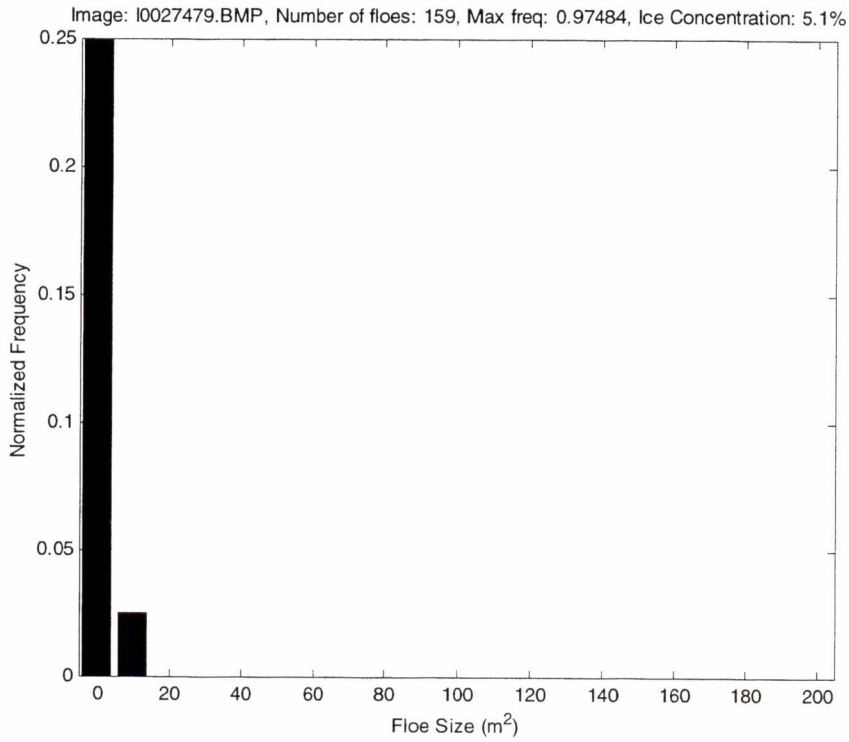


Figure 4.1.6g) Histogram of floe size.

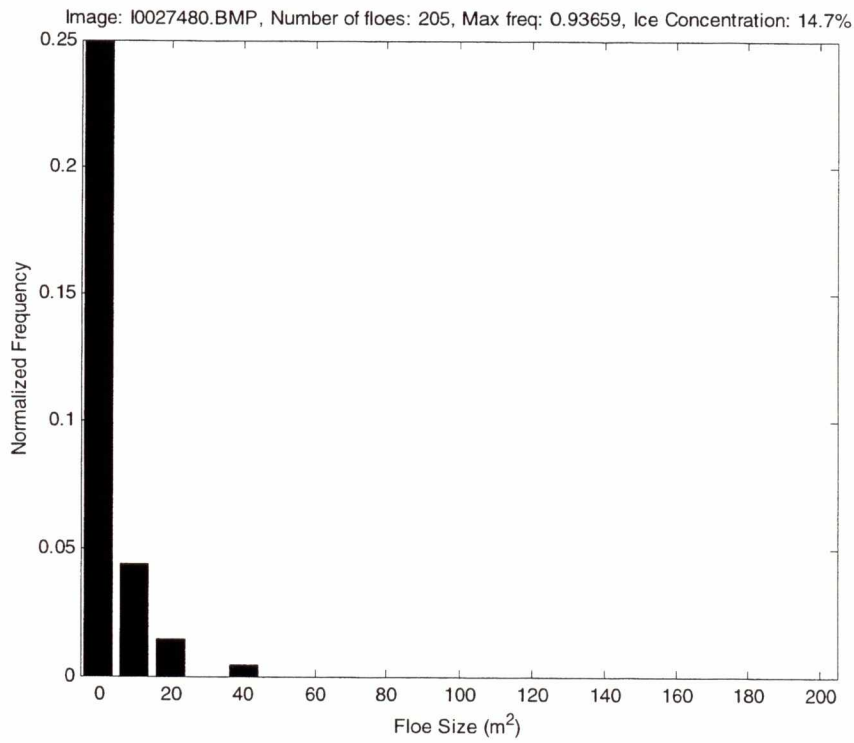


Figure 4.1.6h) Histogram of floe size.

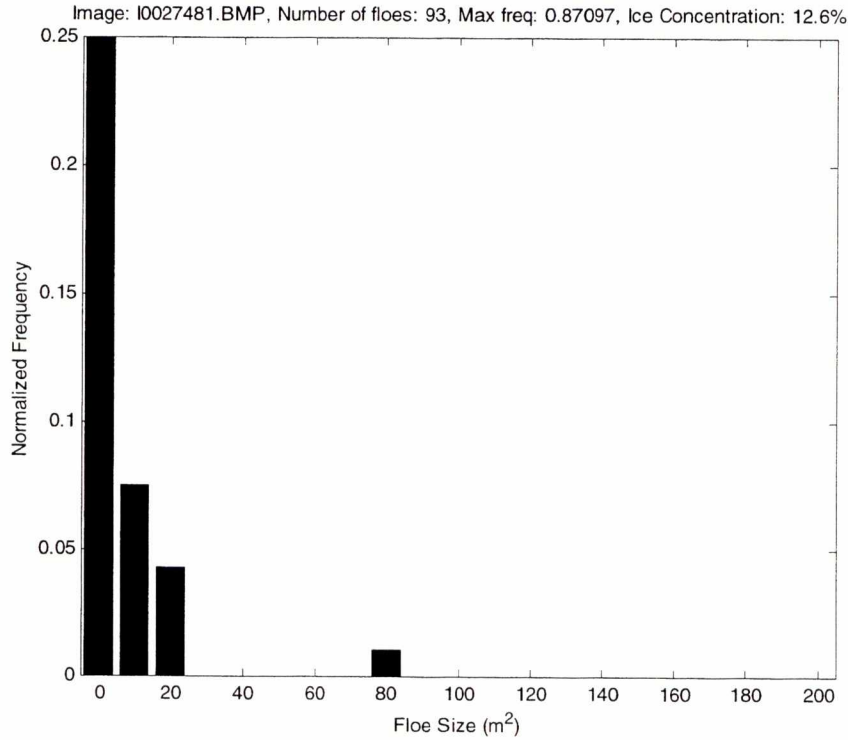


Figure 4.1.6i) Histogram of floe size.

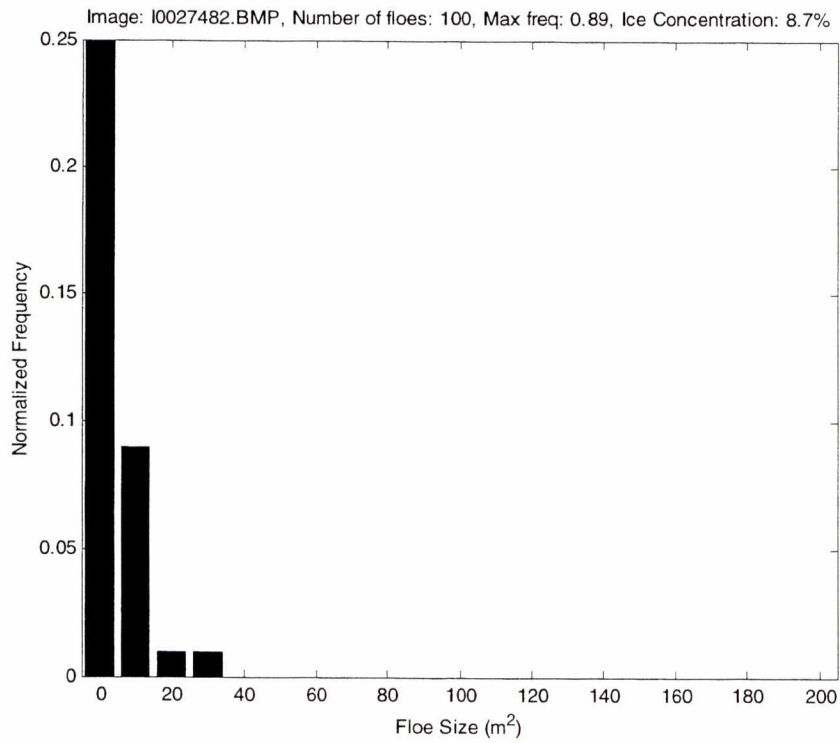


Figure 4.1.6j) Histogram of floe size.

For the automatic processing, a single threshold value was chosen which provided the best results for all ten images. For the manual processing, ice that appeared to be part of a floe was outlined even though the intensity would have been too low to be classified as ice for the automatic processing. For the manual processing, all ice inside the floe was included. The automated processing does not include the area from pixels inside a floe that were below the threshold. For both the manual and automatic processing, floes with 3 or less pixels were not included in the histogram processing.

For the case of the manual measurements, where two or more floes can be seen to be touching each other, each ice feature recognized as a floe would have been measured separately. The automatic technique would measure the area for all floes that touch each other. The histogram shown in Figure 4.1.6c) from the automated floe size processing for image i0027475 shows one floe at 170 m² and one floe each at 50 m², 40 m² and 30 m². The histogram shown in Figure 4.1.4c) for the manual floe size measurements for the same image shows one floe at 120 m² and two floes at 40 m², two floes at 30 m² and one floe at 20 m². Both histograms show one large floe at 200 m².

4.2 ICE CONCENTRATION MEASUREMENT

Ice concentration measurements were made during the ice floe size processing. For the Limex '89 ice concentration measurements (Rossiter *et al.*, 1992), images were binary-thresholded to classify areas of the video frame as either ice or open water. Binary-thresholding is performed on the images in the automatic ice floe size measurement and the total area of ice floes from the connected components analysis provides the same result as counting all the pixels that are classified as ice. The results of the binary-thresholded ice concentration measurements are provided above the automatic floe size histogram plots shown in Figure 4.1.6 a) to j). For comparison purposes, the areas from the manual floe size measurements were added up and then converted to an ice concentration measurement. Table 4.1.1 lists the ice concentration results.

Table 4.1.1 Ice Concentration results

Image number	Binary threshold ice concentration (percentage)	Ice concentration from manual floe outline (percentage)
i0027473	0.6	0.2
i0027474	19.8	20.1
i0027475	33.6	35.7
i0027476	18.4	19.8
i0027477	23.2	26.5
i0027478	16.4	21.3
i0027479	5.1	8.4
i0027480	14.7	17.5
i0027481	12.6	15.3
i0027482	8.7	9.8

4.3 ICE ROUGHNESS MEASUREMENT

Ice roughness measurements are made using the laser altimeter. The laser altimeter data are processed to remove most of the helicopter's height variations leaving fine surface detail. The fine surface detail is processed to provide an estimate of ice roughness. Figure 3.1.1 a) shows a plot of ice roughness from line 132, which was flown on March 17, 1998.

Holladay and Moucha (1998) documents the processing steps to process laser altimeter data for estimates of ice roughness.

Further results of ice roughness processing of data collected in 1998 with the Video Sensor System can be seen in Prinsenber *et al.* (1999) included in Appendix C.

5 CONCLUSIONS AND RECOMMENDATIONS

It has been shown that the data collected from the various sensors in the video system can be aligned for comparative data analysis for scientific studies and for quick post-flight data display for operational use. Parameter extraction using automatic techniques has been demonstrated.

Prior to this analysis project, the primary results from the video system data set were laser altimeter ice roughness information and AVI movies of the video frames. The various analysis techniques demonstrated in this report show that a wide variety of parameters can be extracted from the video sensor system's data set. Preliminary demonstrations have been provided for the following ice parameters:

- Video image brightness of the ice surface provides indirect ice roughness information
- Colour-space analysis of the ice surface for open water or ice cover detection
- Automatic ice floe size and ice concentration measurements

For the items listed above, the demonstrations were performed using either limited data sets (the technique has not been applied to all data collected) or using a data set picked to demonstrate the result using a minimum of pre-processing steps.

Geo-referenced and quick-look plots of the video images have been demonstrated. The quick-look plots can provide the user with the ice conditions along a survey line in a rapid manner. Hard-copy plots can be archived for the entire field season, so that ice conditions can be quickly viewed and compared without the need for a computer to playback the data.

For operational use, a field data viewer can be developed for rapid viewing of the video sensor data. For operational uses, the parameter extraction technique must work quickly with a minimum of operator involvement. The processing technique must work with all data collected and under all ice conditions. The parameters and display techniques that are ready for field display are:

- GPS flight track positions
- Flying height
- Laser ice roughness
- Quick-look video plots
- Geo-referenced video plots.

The following items require further development to make them ready for either scientific or operational use:

- Video frame mosaicking for plots and extracting a brightness profile.
- Video image colour processing for ice cover
- Automatic ice floe size and ice concentration measurements

6 REFERENCES

- Annan, A.P. and J.L. Davis. 1977. "Radar Range Analysis for Geological Materials", Report of Activities, Part B; Geol. Surv. Can., Paper 77-1B, pp.117-124.
- Fink, D.G. and D. Christiansen. 1982. "Electronic Engineers Handbook, Second Edition", McGraw Hill
- Haralick, R.M. and L.G. Shapiro. 1992. "Computer and Robot Vision Volume 1", Addison Wesley Longman, 608 p.
- Holladay, J.S. and R. Moucha. 1998. "Electromagnetic/Laser Ice Thickness Data from the Labrador Shelf, 1994", Can. Contract. Rep. Hydrogr. Ocean Sci. 49: viii + 340 p.
- Holladay, J.S. and S.J. Prinsenber. 1999. "Airborne Electromagnetic Sea Ice Sounding Measurements during 1998 Gulf of St. Lawrence Field Program", Can. Contract. Rep. Hydrogr. Ocean Sci. 53: vi + 118 p.
- Prinsenber, S.J., I.K. Peterson and L. A. Lalumiere. 1999. "Video/laser Helicopter Sensor to Collect Pack Ice Properties for Validation of Radarsat SAR Backscatter Values", Proceedings of the 15th international conference on Port and Ocean Engineering under Arctic conditions, POAC'99, Helsinki, August 23-27, 1999. Volume 1: 285-293.
- Rossiter, J.R., J.S. Holladay and L.A. Lalumiere. 1992. "Validation of Airborne Sea Ice Thickness Measurement Using Electromagnetic Induction During Limex 89", (UP-C8-028). Can. Contractor Rep. Hydrogr. Ocean Sci. 41: x + 61 p.
- Sensors by Design, Ltd. 1998. "Winter 1998, BIO Video Sensor System, Field and Data Report", Internal Report for Fisheries and Oceans, Bedford Institute of Oceanography, DSS Contract #F5955-7-0329, 21 p.

Appendix A Video Distortion Correction Example

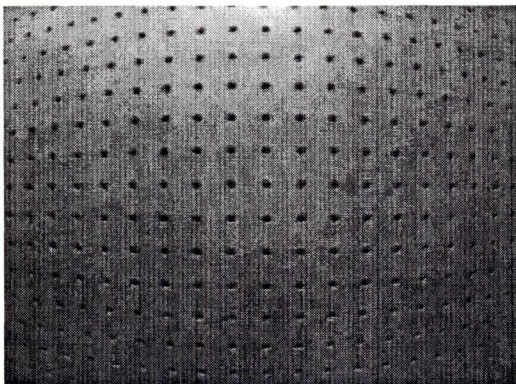
The video sensor system has been flown with a 6 mm lens and a 4.2 mm wide-angle lens. The horizontal field of view is 56 degrees for the 6 mm lens and 75 degrees for the 4.2 mm lens. The wide-angle lens has considerable distortion which is most noticeable when the video frames are played back in an AVI movie.

This test used a fairly coarse grid pattern for the correction. As a result, approximately 10 % of the image width is lost when the correction is applied to correct image distortion. With 10% loss, the corrected wide-angle image is still 20% wider than an image collected with the 6 mm lens. The corrected airborne image example shown below has been cropped to remove the edge distortion.

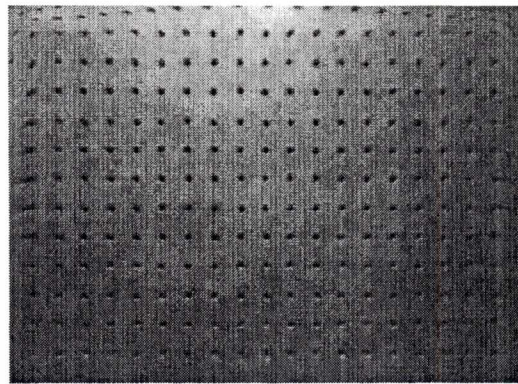
For operational use the correction factors should be calculated with a finer grid. Lighting of the grid surface should be more uniform to make locating the grid points simpler. Locating the grid points should be performed with as high a precision as possible.

Correction-Factor Image

Source Image

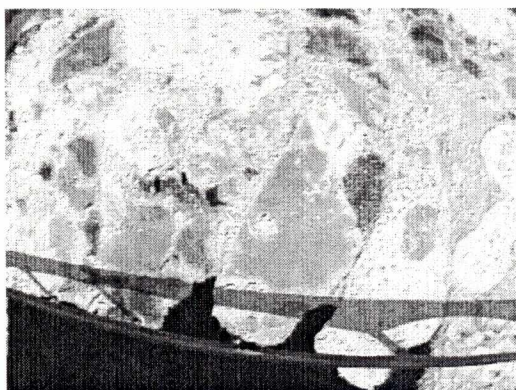


After Correction

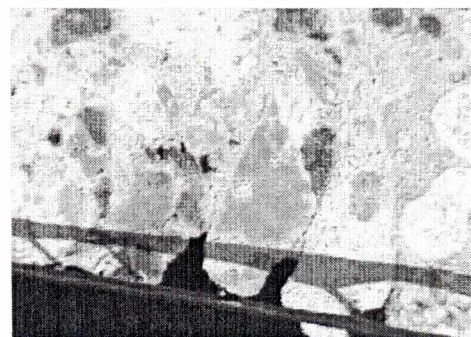


Example airborne image before and after correction

Original Survey Image



After Correction



Appendix B Laser Pointer Method for Laser Altimeter/Video Alignment

Prior to the 1999 field trial a calibration technique was developed to locate the point in the video images where the laser altimeter was ranging to. As laser altimeter uses invisible near infrared light it must be detected using a device such as the Radio Shack 286-1099 Infrared Sensor card.

A small laser pointer (Merangue LP08B4BX) was mounted to the side of the Optech G-150 laser altimeter. The laser was placed 10 away from a wall, and in the dark, the beam's position was located using the infrared sensor card and marked on the wall. The laser pointer was then turned on and its position was marked on the wall. A video frame was captured showing the bright point-sized light of the laser pointer on the wall. The pixel location of the laser pointer can be located in the image and the position of the laser altimeter can be estimated by simple geometry.

Laser Beam Width

The Infrared card was held 3.4 m from the laser altimeter and the laser's beam width was estimated. The horizontal beam width was found to 45 mm (at 3.4 m range) and the vertical beam width was 30 mm.

Appendix C. (paper from POAC'99, Volume 1: 285-293).

**VIDEO/LASER HELICOPTER SENSOR TO COLLECT PACK ICE PROPERTIES
FOR VALIDATION OF RADARSAT SAR BACKSCATTER VALUES**

S.J. Prinsenber¹, I.K. Peterson¹ and L. Lalumiere²

¹Bedford Institute of Oceanography, Dartmouth, Nova Scotia, Canada.

²Sensors by Design Ltd., Newmarket, Ontario, Canada.

ABSTRACT

A helicopter-mounted Video-Laser-GPS system was used to collect video images and surface roughness data from the Gulf of St. Lawrence pack ice to validate the effect of the pack ice properties on the RADARSAT backscatter values in the RADARSAT ScanSAR Wide images. As ice floes become smaller than the pixel size (50m) of the RADARSAT ScanSAR Wide image, the pixel backscatter properties not only depend on ice properties but also on the fraction of open water within the pixel. To study the dependence of the SAR backscatter on ice concentration as well as on the floe size distribution and surface roughness, the video/laser data was collected from pack ice areas with different backscatter values. GPS-ARGOS ice beacons deployed on ice floes provided hourly ice velocities to co-register the imagery with the helicopter-borne sensor data. Two SAR image examples are shown; one from Northumberland Strait of February 20, 1998 when the backscatter properties of the pack ice were deformed by the Bridge piers. The second example is from the marginal ice zone of March 13, 1998 where dynamic processes affect the sub-pixel roughness and ice concentration of the pack ice.

1. INTRODUCTION

Winter navigation in Canadian waters relies heavily on ice information that can be extracted from remotely sensed data especially RADARSAT SAR imagery, as ice reconnaissance flights by fixed-wing or helicopter are costly, weather dependent and spatial restrictive. To improve the interpretation of RADARSAT SAR imagery, reconnaissance flights are necessary to collect ground-truth ice property data. In Canada, helicopter-borne sensors have been developed to optimize both the quality and quantity that can be collected during helicopter reconnaissance flights.

One such sensor is an electromagnetic (EM) induction system (Rossiter and Holladay, 1994) which collects snow-plus-ice thickness and surface roughness data. Results of its uses in Radarsat validation are reported in Peterson et al. (1999, this issue). The other sensor is a Video-Laser-GPS system that is capable of collecting floe size distribution, ice concentration and surface roughness data. This note will describe the data collected by this second sensor during the winter of 1998 in the southern Gulf of St. Lawrence.

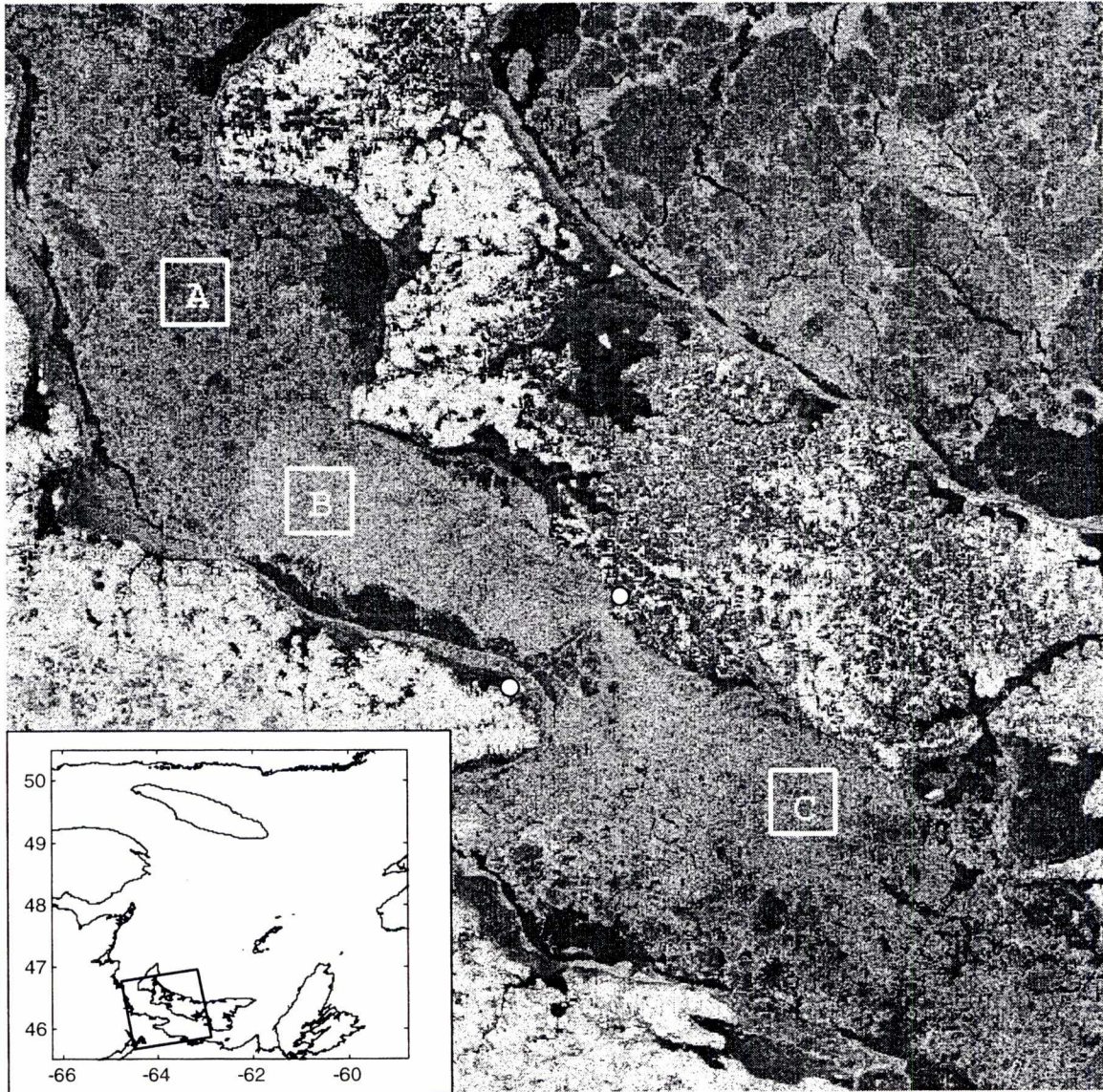


Figure. 1. RADARSAT ScanSAR Wide sub-scene acquired in February 20, 1998 (22:08Z) showing Northumberland Strait. The inset shows the area of the southern Gulf of St. Lawrence covered by the image. © CSA/ASC, 1998.

2. FIELD SURVEY

In February-March 1998, a field program was conducted out of Charlottetown, Prince Edward Island (P.E.I.) to collect ice property data to validate signatures seen in the RADARSAT SAR imagery from the southern Gulf of St. Lawrence. Some of the survey work was done south of P.E.I. in Northumberland Strait where the 13km long Confederation Bridge has recently been completed (narrow section of the strait, linking the two white dots in Figure 1). The Video system frame-grabs digital video images and logs laser altimeter profiles along with GPS position data. The system uses the expected flying height, flying speed, field of

view and frame size to establish the frame capture rate which ranges from 0.5sec when flying at 50m to 3.0sec at 300m (1000ft). Since the video frame has 240x320 pixels and the video frame view width is approximately equal to the flying height, the video pixel size is about 15cm when flying at 50m and 1m when flying at 300m. GPS data are logged at 1/sec, radar altimeter at 10/sec and laser altimeter at 30/sec. ARGOS satellite-tracked GPS ice beacons were deployed on ice floes to monitor ice drift. Hourly GPS-derived position data from the beacons were telemetered via Service ARGOS and have an accuracy of about 40m.

3. RESULTS

The February 20 image shows that west of the bridge there exists an ice area with a high backscatter value which changes abruptly to low values when pack ice with floe sizes of 2 to 5km is encountered. The bridge piers cuts the pack ice into small floes (10 - 100m), as the ice moves back and forth past the bridge in response to tidal currents and wind forcing (Peterson et al., 1998a). The ice area affected by the bridge piers was monitored by satellite-tracked ice beacons which indicated that the pack ice moved 40km to the west under strong easterly winds from February 18 to 20 (Figure 2). Two beacons were placed west of the bridge on large floes unaffected by the bridge piers, while the other two beacons were placed east of the bridge on small floes already affected by the bridge piers. The area between the two pair of beacons thus track the demarcation line between large and small floes, which at the time of the image was 40km east of the Bridge.

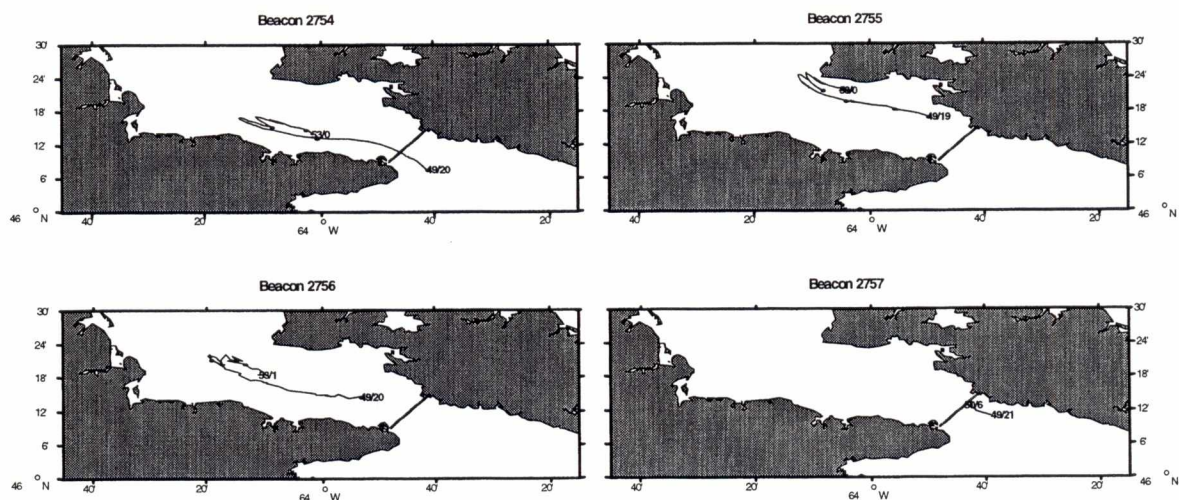


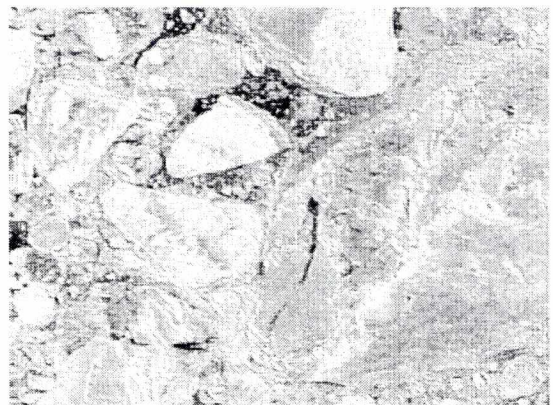
Figure 2. Beacon trajectories between day 49, Feb. 18 (19:00-21:00AST) and day 53, Feb. 22 (01:00AST). Tidal ice motion is seen in trajectories of beacons #2754 and #2755. Beacon #2757 sunk while passing the bridge area on day 50 (06:00AST)

The relative brightness (grey level) of the image changes from 50 of the unaffected pack ice (area A on Figure1) to 69 for the affected area west of the bridge where small, rough floes are present (area B) and back to 62 for the area C east of the bridge where the small floes possibly occur at a lower ice concentration.

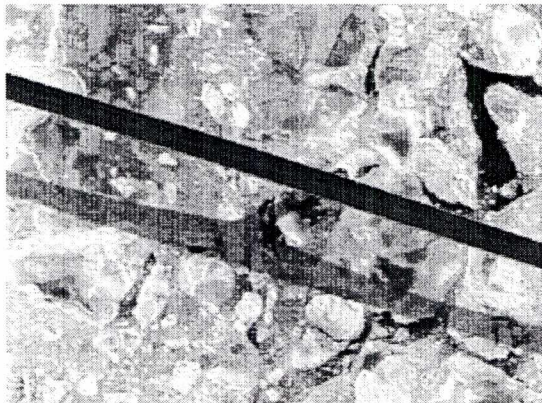
The different backscatter brightness in RADARSAT imagery near the bridge is related to sub-pixel scale properties seen in the video images acquired on February 24 (Figure 3) while flying at a height of 200m along the Strait from west to east. Before the affected area west of the Bridge was reached large floes encompassed the entire video image (#2285). The ice in the other three images of Figure 3 is of same general ice type but has been fractured by the piers of the bridge; brash ice has also been produced in the open water areas between the floes.



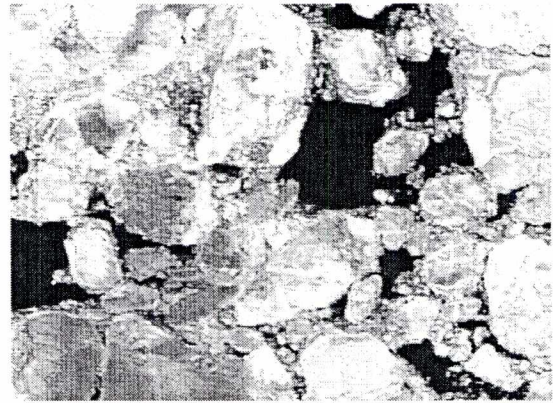
#2285 (11:05)



#2410 (11:11)



#2556 (11:18)



#2700 (11:25)

Figure 3. Video images from February 24, 1998 between 11:05AST and 11:25AST. The horizontal scale of the images is approximately 200m; equal the video height.

Video image #2410 is from west of the Bridge and #2700 from east of the Bridge. Image #2556 shows the image while passing over the bridge. When the small floes occur in high ice concentration (#2410), the brightness in the RADARSAT image increases relative to unaffected areas (#2285). As more open water appears between

the small floes (#2700), the backscatter decreases as low backscatter from the water (light winds) nullified the increase in backscatter due to rough floe topography. The laser was not yet installed at this time of the survey, and thus no laser roughness data is available.

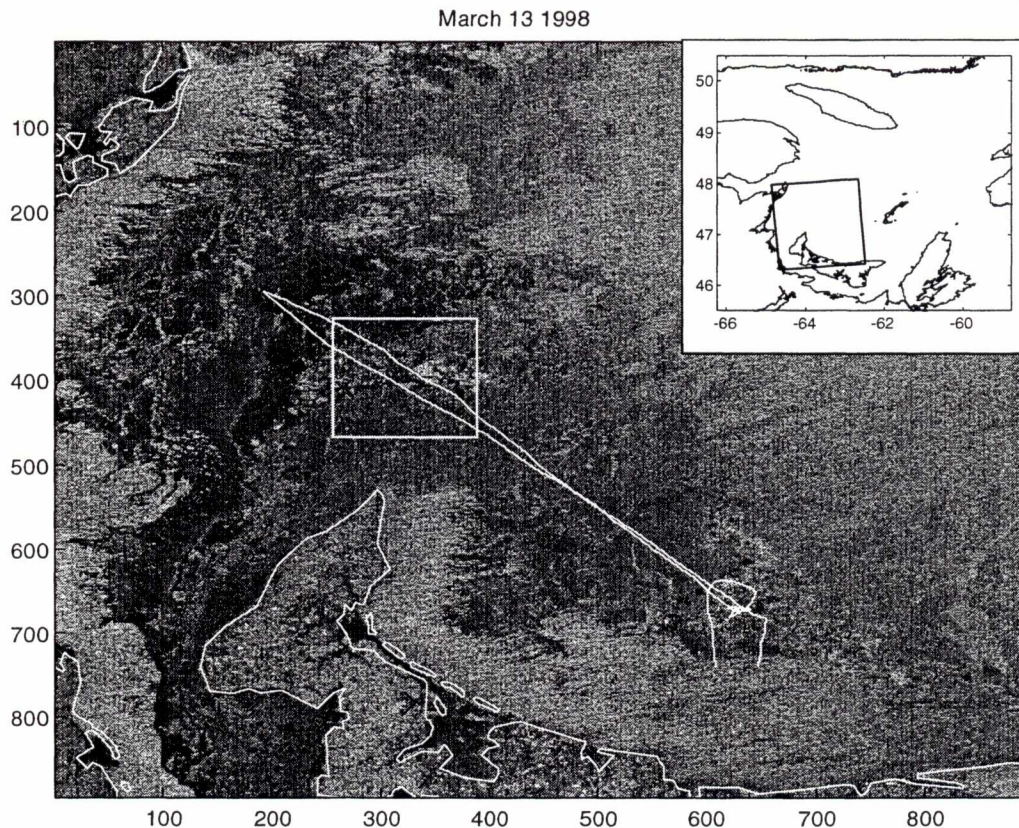


Figure 4. RADARSAT ScanSAR Wide scene from March 13, 1998 (21:57Z) covering the area north and northwest of PEI. The inset shows the area of the Gulf of St. Lawrence covered by the image and the rectangular sub-scene section shown in Figure 5. © CSA/ASC, 1998.

In the marginal ice zone, the small scale variation in pack ice roughness and ice concentration are caused by dynamic processes as the pack ice grows or decays. The RADARSAT image of March 13, 1998 (Figure 4) shows the video flight path that extended from the first year ice north of PEI, into the ice edge NW of PEI where smooth, new ice areas (dark areas on image) were encountered. Between the first year ice and the new ice area, the flight path passed over brash ice and some deformed floes (bright on the image).

A sub-scene (Figure 5) shows the section of the flight path that passed over the bright image areas. The flight path was moved ESE by 2.9km for the estimated ice drift over the 1.5hr time difference between the SAR and video images. The ice drift was based on data from a GPS ice beacon about 7km east of the flight track. The

pack ice roughness data collected by the laser at 50m altitude and the SAR brightness from the image along the track are shown in Figure 6. There is good agreement between the degree of surface roughness and the SAR brightness.

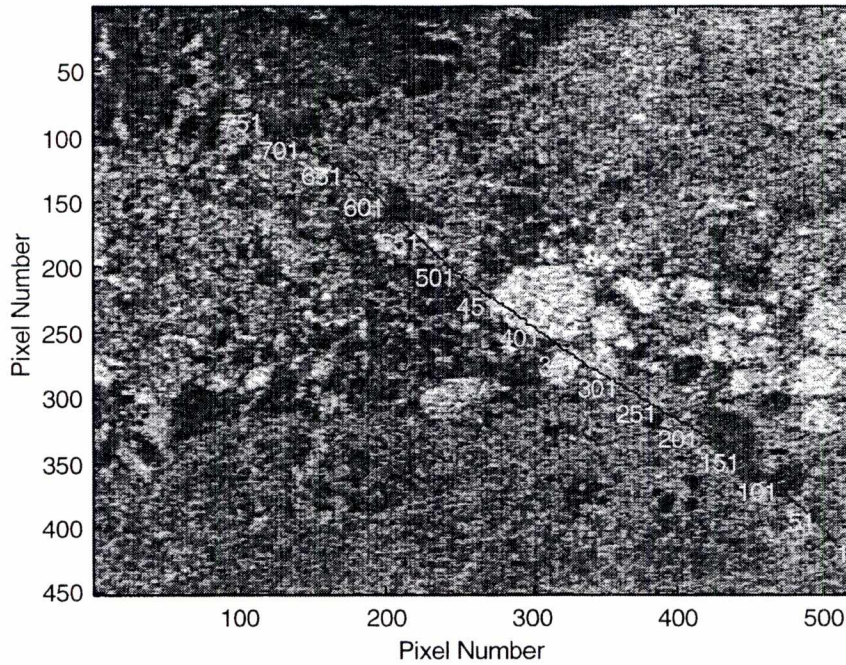


Figure 5. RADARSAT ScanSAR Wide sub-scene from March 13, 1998 (21:57Z) for a 25kmx20km area with video numbers along flight track. © CSA/ASC, 1998.

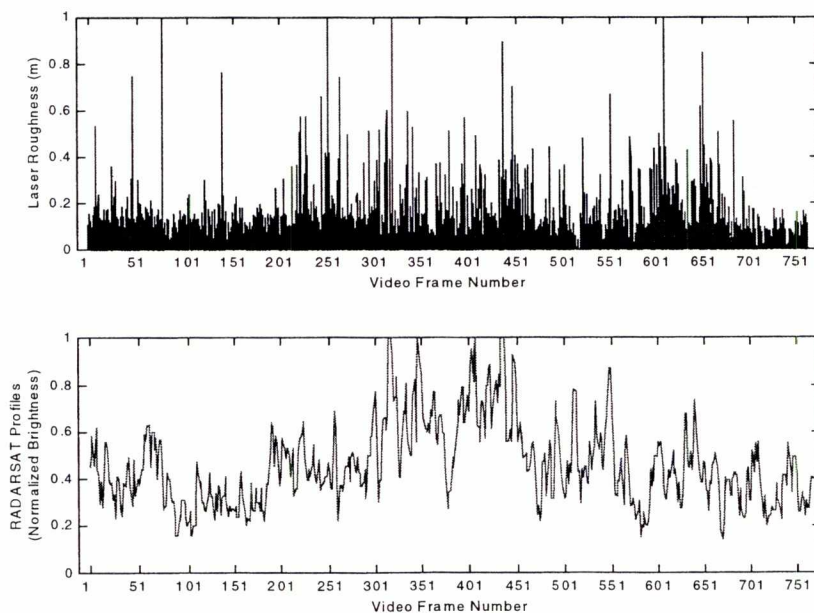
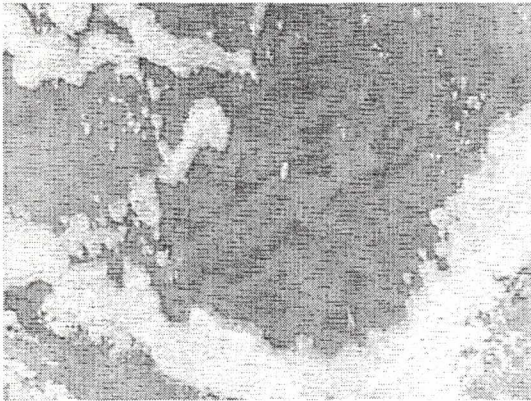
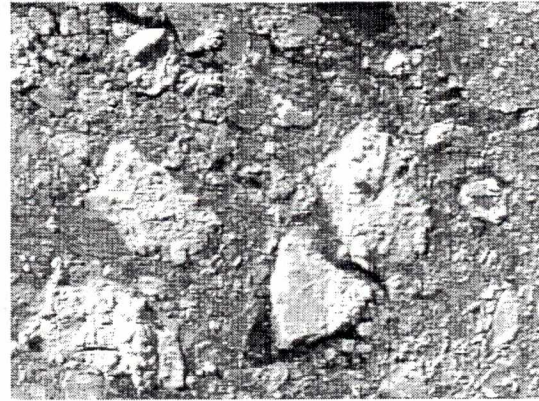


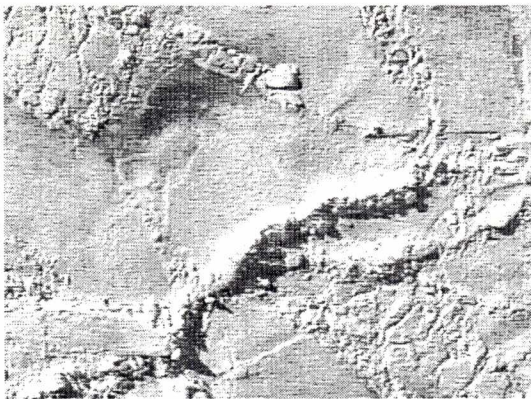
Figure 6. Laser roughness and RADARSAT brightness profiles along the track shown in Figure 5, flown on March 13, 1998 between 20:20Z and 20:29Z.



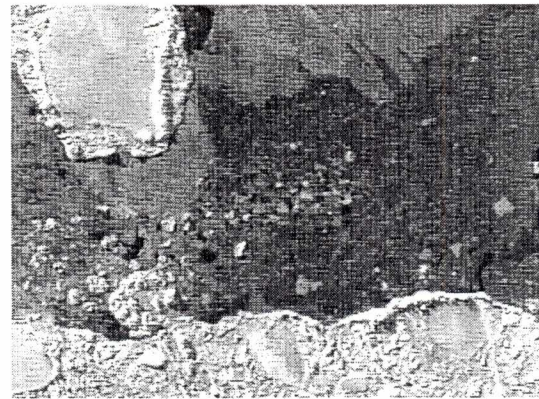
#108



#287



#435



#678

Figure 7. Video images from March 13, 1998 between 20:20Z and 20:29Z. The horizontal scale of the video is approximately 50m; equal the video height.

The darker areas along the track at the start (video images 75-190) and at the end of the track (video images >700) are from the smoother ice areas along the track. In contrast, the high roughness areas are associated with the brighter areas of the SAR image. In Figure 7, four examples are shown of the different ice properties along the track. The smooth level ice shown in image #108 is from the dark area (Figure 5) at the start of the track where low roughness values were observed by the laser (Figure 6). Video #287 represents the grey area of the SAR image and shows a mixture of brash ice and small rough floes. The brightest areas along the track represent rough, rafted and ridged ice (image #435), consolidated into large floes (100% ice concentration). Ridging is most pronounced near the edges of the floes. Image # 678 shows the rough-to-smooth ice transition area with the younger and smoother ice farther along the track to the northeast.

Presently the video data is stored as a colour image consisting of three 8-bit colour planes. Investigation is underway to determine what information will be lost if either the colours are combined in one single grey scale or if just one of the

colour plane is retained. Figure 8 shows the four available grey scale images of the image #287 shown in Figure 7. The combined grey scale is the sum of 0.299(red plane), 0.587(green plane) and 0.114(blue plane). It follows the sensitivity of the eye, which is most sensitive to the green part of the colour spectrum. One concern is that when one develops an automatic image analysis routine to determine such things as ridge frequencies and ice concentrations of various ice types, will shadows be properly identified as ice rather than as thin ice or open water. Figure 8 shows that the Blue colour plane does distinguish the thin ice types the best from either the open water area (black) or from shadow areas (light grey). However ridges become less distinguishable in the blue colour plane than in any other colour or combine grey scale planes. For this example, the red colour plane appears the best plane to provide ridge information. One colour grey plane may thus not provide all the required information.

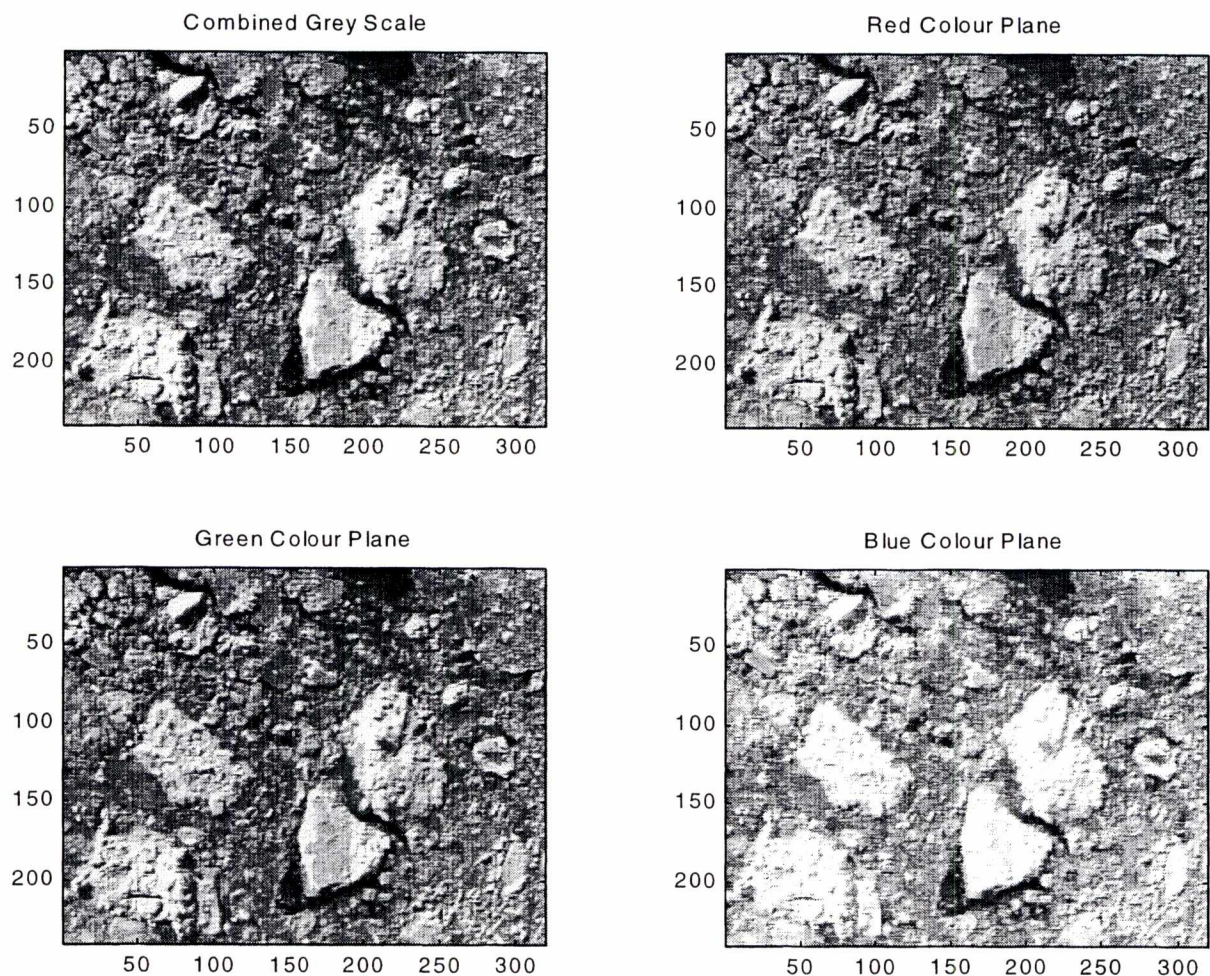


Figure 8. Video image #287 (Figure 7) plotted as a grey scale version using a combined grey scale and the red, green and blue 8-bit colour planes.

4. CONCLUSION

Video and laser data collected by the GPS-Video-Laser system show that for the same ice type, the ice concentration and ice roughness affects the brightness of the SAR backscatter with brighter areas of the pack ice associated with rougher and higher ice concentration for each pixel of the RADARSAT image. Floes fractured by bridge piers that are smaller than the ScanSar Wide pixel scale do occur in high ice concentration in Northumberland Strait and causes high back scatter values. Within the pack ice convergence causes ridging and rafting which when consolidates into large floes will have high backscatter values due to the high surface roughness. New and young ice, which formed in nearby open water areas, had low backscatter values due to low surface roughness as the ice formed during calm winds (no pancake ice). The GPS-Video-Laser system provides valuable data to validate ice signatures in SAR RADARSAT imagery; the tasks in hand now is to develop analysis techniques to extract useful ice information from the data in near real-time that can be made available to the marine shipping industry.

5. ACKNOWLEDGEMENTS

This work was funded in part by the Federal Panel on Energy Research and Development. We thank Andy Maillet of the Can. Coast Guard, our colleagues from the Bedford Institute, and other participants of the project from the Canadian Coast Guard, Transport Canada, Canadian Ice Service and Canada Centre for Remote Sensing.

6. REFERENCES

- Peterson, I.K., Prinsenber, S.J. and Maillet, A. 1998. 1997 Pack ice properties in Northumberland Strait. ISOPE'98: Proceedings of the 8th International Offshore and Polar Engineering Conference, Montreal, Canada, Vol. 2, pp. 513-518.
- Peterson, I.K., Prinsenber, S.J. and Holladay, J.S. 1999. Using a helicopter-borne EM-induction system to validate RADARSAT sea ice signatures. Proceedings of 15th International Conference on Port and Ocean Engineering under Arctic Conditions, POAC'99, Helsinki, Finland, this issue.
- Rossiter, J.R. and Holladay, J.S. 1994. Ice-thickness measurement. In: Remote Sensing of Sea Ice and Icebergs. John Wiley and Sons, New York, pp. 41-176.